Analytic three-dimensional primary hair charged black holes with Coulomb-like electrodynamics and their thermodynamics

Ayan Daripa* and Subhash Mahapatra†

Department of Physics and Astronomy, National Institute of Technology Rourkela, Rourkela—769008, India

(Received 16 January 2024; accepted 22 May 2024; published 14 June 2024)

We construct and discuss new solutions of primary hair charged black holes in asymptotically anti–de Sitter space that have well-defined Coulomb-like potential in three dimensions. The gauge field source to the Einstein equation is a power-Maxwell nonlinear electrodynamics with traceless energy-momentum tensor. The coupled Einstein-power-Maxwell-scalar gravity system, which carries the coupling $f(\phi)$ between the gauge and scalar fields, is analyzed, and hairy-charged black hole solutions are found analytically. We consider three different profiles of the coupling functions: (i) $f(\phi) = 1$, corresponding to no direct coupling between the gauge and scalar fields, (ii) $f(\phi) = e^{\phi}$, and (iii) $f(\phi) = e^{\phi^2/2}$, corresponding to their nonminimal coupling. For all these cases, the scalar field, gauge fields, and curvature scalars are regular and well behaved everywhere outside the horizon. We further study the thermodynamics of the obtained hairy black hole in the canonical and grand-canonical ensembles and find significant changes in its thermodynamic structure due to the scalar field. In particular, for all considered coupling functions, the hairy parameter has a critical value above which the hairy black hole undergoes the Hawking/Page phase transition, whereas below which no such phase transition appears.

DOI: 10.1103/PhysRevD.109.124039

I. INTRODUCTION

For many years, physicists and astronomers have been fascinated by the black hole mysteries and their fascinating nature. The study of black holes gives a unique platform to view the behavior of matter and energy under extreme circumstances and provides insights into basic principles of general relativity. They offer a unique framework for the coexistence of strong gravity, quantum phenomena, and thermodynamics. It is now widely accepted that black holes carry both temperature and entropy and may experience phase transitions much as ordinary thermodynamic systems [1–3]. For instance, in contrast to the Schwarzschild black hole in asymptotically flat space, black holes in anti–de Sitter (AdS) spaces are not only thermodynamically stable but also exhibit rich thermodynamic phase structures and go through phase transitions such as the Hawking/Page (black hole to thermal-AdS) or the small/large black hole phase transitions [4–11].

Owing to their intrinsic simplicity compared to their higher-dimensional counterparts, studies of lower-dimensional gravitational systems have drawn a lot of interest. The prime example is the three-dimensional Banados-Teitelboim-Zanelli (BTZ) black holes, which have received a lot of attention in the last three decades and have shown to be useful simplified models for investigating conceptual issues of black holes [12,13]. For example, general relativity becomes a topological field theory in the three dimensions, whose dynamics can be mapped holographically to the two-dimensional conformal field theory (CFT) living at the boundary of spacetime [14]. The BTZ black holes, therefore provide a natural arena to test the deep and fundamental principles of gauge/gravity duality [15]. The use of conformal boundary conserved charges and symmetric algebra to calculate the entropy of BTZ black holes provides a prime example of the usefulness of lower-dimensional gravity systems to get possible insight into quantum gravity [16]. In addition, the Chern-Simons formulation of three-dimensional gravity models has made them quintessential for investigating general properties of gravity, and in particular its relationship with gauge field theories [17,18]. Indeed, despite having various contrasting features compared to their higher-dimensional counterparts—such as not containing any curvature singularity or being locally equivalent to pure AdS_3—the BTZ black holes do exhibit many of their fundamental features, such as the presence of event and Cauchy horizons, or their thermodynamic and holographic interpretations [19]. For these reasons, the lower-dimensional models continue to be the focus of considerable interest in gravitational theories [20,21].

The repertory of three-dimensional black hole solutions has greatly broadened in a number of ways since the

*ayandaripaadra@gmail.com
†mahapatrasub@nitrkl.ac.in

seminal discovery of the BTZ solution. In addition to the traditional Maxwell term [22], higher-order curvature terms [23], higher-rank tensor fields [24], gravitational Chern-Simons terms [25], etc. have been added in the gravity action. The extension also includes a variety of other matter sources. These advancements have improved our knowledge of lower-dimensional black hole solutions and their interactions with various types of matter. The Maxwell Lagrangian, $\mathcal{L}(\mathcal{F}) = \mathcal{F} = F_{\mu\nu}F^{\mu\nu}$, in particular, leads to an interesting but undesirable behavior in three dimensions, i.e., the electric field and potential of the black hole are now proportional to $1/r$ and $\log r$ respectively, r being the radial coordinate, as opposed to $1/r^2$ and $1/r$ behavior in four dimensions. Consequently, divergence terms appear in the metric and gauge field, as $\log(r)$ blows up at $r = 0$ and $r = \infty$, making the charged BTZ solution unattractive. This raises the potential question: is it possible to construct a Lagrangian for the gauge field that will give us a gauge field solution just like in the case of $(3 + 1)$ dimensions, i.e., a regular and well-behaved gauge field solution? This question was addressed in [26], where the answer was found in the affirmative. The essential idea was to require, as in four dimensions, the trace of the gauge field energy-momentum tensor to be zero. This condition uniquely constrained the gauge field Lagrangian to be powerlike with exponent $3/4$, i.e., for the power law Lagrangian $\mathcal{L}(\mathcal{F}) = (s\mathcal{F})^p$, the trace

$$T = T_{\mu\nu}g^{\mu\nu} = 3\mathcal{L}(\mathcal{F}) - 4\mathcal{F}\mathcal{L}_{,\mathcal{F}} = \left(\frac{3}{2} - 2p\right)(s\mathcal{F})^p$$

vanishes for the exponent value $p = 3/4$. It is straightforward to check that this traceless nonlinear electrodynamics $[\mathcal{L}(\mathcal{F}) = (s\mathcal{F})^{3/4}]$ causes the radial dependence of electric field and potential to be $1/r^2$ and $1/r$ in $(2 + 1)$ dimensions, respectively. Moreover, this energy-momentum tensor also fulfils the weak energy conditions. Adding this nonlinear Lagrangian to the Einstein-Hilbert action further gives three-dimensional black hole solutions with finite gauge field everywhere [26], unlike the usual charged BTZ black hole [22]. Subsequently, several works have investigated various properties of these $(2 + 1)$-dimensional black holes with a Coulomb-like field [27–45].

In a similar vein, numerous hairy black hole solutions involving self-interacting real scalar field, both minimally and nonminimally coupled, have been investigated in three-dimensional spacetime following the initial work of [46,47]. The investigation of the interplay between scalar fields and black holes in three dimensions has not only improved our understanding of the interaction between them but also has opened up a wide range of their potential applications, especially in the context of AdS spaces, i.e., the scalar-gravity models are very pertinent to holography and are useful resources for studying lower-dimensional condensed matter systems at strong couplings. The desirable trait of analytical tractability of three-dimensional scalar gravity models has also greatly piqued our curiosity [48–65]. Nonetheless, it should be emphasized that not all scalar field-dressed black hole solutions obtained in three dimensions have desirable physical properties. In many cases, the scalar field not only shows logarithmic radial dependency, thereby making them unsatisfactory but also the geometry does not asymptote to AdS at the boundary [57,61].

Another important reason for greatly investigating scalar-gravity systems is due to their connections with the no-hair theorem. The no-hair theorem basically asserts that black holes in the asymptotically flat spaces are uniquely described by their mass, charge, and angular momentum [66]. Many strong arguments and critical remarks in favor of the no-scalar hair theorem for asymptotic flat spacetime were discussed in [67–69], and have long been thought to apply to black holes in general. For a review on the issue of scalar hair in asymptotic flat spaces, see [70]. While multiple subsequent investigations have endorsed the original no-hair theorem for black holes [71–77], it is crucial to keep in mind that it is not a theorem in the strict mathematical sense. Many counterexamples have contested the no-hair theorem over time. The Einstein-Yang-Mills theory [78,79], dilatonic black holes [80], black holes with Skyrme hairs [81], and black hole hair with tensor vacuum [82,83] are a few instances of these counterexamples.

The analytical tractability of scalar gravity systems in three dimensions have made them great laboratories for discussing the no-hair theorem [27]. It is then natural to construct and investigate analytic scalar hair black hole solutions with a well-behaved Coulomb-like structure for the gauge field using the Einstein-power Maxwell-scalar gravity system. Such solutions have been obtained in relatively few systems [84–87]. However, the scalar field in these hairy solutions depends logarithmically on the radial coordinate and therefore, diverges at the boundary. Moreover, the solutions do not asymptote to AdS at the boundary, thereby severely restricting their potential applicability.

From the thermodynamic perspective as well, the scalar hair can change the thermodynamic phase structure of three-dimensional black holes considerably. In particular, the black hole temperature exhibits multiple branches in four and higher dimensions, allowing for the possibility of phase transitions as the temperature varies. Two prominent examples of such phase transitions are the Hawking/Page phase transition between AdS black holes and thermal-AdS in the grand canonical ensemble and the liquid/gas type phase transition between small and large black holes in the fixed charge ensemble, whereas the temperature profile in BTZ black hole exhibits only one branch, displaying no phase transitions in both charged and uncharged cases. However, recently, it was observed that certain three-dimensional hairy black holes, obtained from the potential reconstruction technique, can exhibit such phase transitions

in the presence of nontrivial primary scalar hair [88]. In particular, it was observed that depending on the coupling function $f(\phi)$ between the gauge and scalar field, the primary scalar hair can greatly influence the phase structure of three-dimensional black holes and resemble them to that of higher-dimensional charged AdS black holes.

Since the addition of scalar and gauge fields to Einstein's gravity usually generates unexpected and exciting features in black hole solutions, it is instructive to find new exact solutions to the Einstein-power Maxwell-scalar gravity system for arbitrary coupling functions and investigate how the geometrical and thermodynamical properties of black holes are altered in the presence of a scalar field. In particular, it is interesting and desirable to have three-dimensional primary hair black hole solutions, with not just a regular profile of the scalar field but also of the gauge field, as such solutions might have applications in applied holography. For instance, such solutions can be useful in the context of $(1+1)$-dimensional holographic superconductors [89,90][1]; regular gauge field solutions could also be important for holographic Fermi-Luttinger liquids and Friedel oscillations in two dimensions [91–93]. Such regular field solutions might also play an important role in investigating two-dimensional QCD, where the scalar field plays the role of a running coupling constant in the dual theory [94].[2] This can be important from a theoretical perspective as well since two-dimensional QCD has been suggested to be equivalent to a string theory [95].

This paper introduces analytical charged primary hair black hole solutions in three dimensions with a power Maxwell field, whose thermodynamic structure is somewhat similar to that of charged AdS black holes in higher dimensions. We focus on the Einstein-power Maxwell-scalar gravity system, which has a coupling function $f(\phi)$ between the scalar and power Maxwell fields, and use the potential reconstruction technique [94,96–106] to simultaneously solve the coupled Einstein-power Maxwell-scalar field equations in terms of functions $f(\phi)$ and $A(z)$ (see the next section for details). The different forms of $f(\phi)$ and $A(z)$ then allow us to construct a different family of hairy black hole solutions. To make the analysis and findings more thorough, we choose three different but physically motivated forms of the coupling function: (i) $f(\phi)=1$, (ii) $f(\phi)=e^{\phi}$, and (iii) $f(\phi)=e^{\phi^2/2}$. While the second and third coupling functions relate to a nonminimal coupling between the scalar and gauge fields, the first coupling function indicates that there is no direct coupling between them. The primary reason for taking into account such coupling functions is the fact that they have recently been thoroughly investigated in a variety of higher-dimensional hairy black hole contexts, from scalarization to holographic model construction [107], and have consistently contributed to our understanding of the hairy aspects of black holes. Therefore, it is intriguing to look into how these coupling functions affect the geometrical and thermodynamical features of three-dimensional black holes as well. We similarly take a particularly simple form of $A(z)=-a^2z^2$, which enables us to introduce the parameter a, which regulates the strength of the scalar field.

For all forms of $A(z)$ and $f(\phi)$ considered here, the found hairy black hole solutions exhibit many attractive features. This includes that (i) the scalar field is finite and well-behaved everywhere in the outer horizon region and falls off at the asymptotic AdS boundary; (ii) the gauge field is also finite everywhere outside the horizon; (iii) the curvature scalars, such as the Kretschmann and Ricci scalars, are also finite everywhere outside the horizon, suggesting no additional singularity in the hairy solution than those already present in the nonhairy case; (iv) these hairy solutions can be analytically continued to standard BTZ solution in the limits $\{a\to 0, q_e\to 0\}$; and (v) the potential is bounded from above from its UV boundary value, thereby satisfying the Gubser criterion to have a well-defined boundary theory [108].

We then analyze the thermodynamic structure of the obtained hairy solutions in the canonical and grand-canonical ensembles and find that it changes significantly when the hairy parameter a is turned on. In particular, for all considered coupling functions, and in both canonical and grand-canonical ensembles, a critical value of the hairy parameter $a=a_c$ appears (which is a $f(\phi)$ dependent quantity) above which the hairy black hole undergoes the Hawking/Page phase transition to thermal-AdS phase, whereas no such phase transition appears below a_c. For the uncharged $q_e=0$ case, the Hawking/Page phase transition exists for all finite values of a. The corresponding transition temperature also increases monotonically with a. Moreover, the critical value a_c turns out to be a μ_e and q_e dependent quantity in the grand-canonical and canonical ensembles respectively, i.e., its magnitude increases as μ_e or q_e increases. This thermodynamic behavior of the hairy black hole is therefore analogous to the BTZ black hole for $a<a_c$ whereas it resembles the RN-AdS black hole in the grand-canonical ensemble for $a>a_c$. Moreover, we find that these primary hair black holes are also thermodynamically stable as they exhibit positive specific heat.

At this point, we would like to mention that our hairy solutions correspond to the primary hair. One should in principle distinguish primary hair from secondary hair [109]. The secondary hair refers to black hole structures

[1]Unlike our gravity model, the scalar field is usually charged under the U(1) gauge field in holographic superconductors. However, charged AdS black hole can also become unstable to form neutral condensate [89].

[2]A different metric Ansa$\ddot{a}$tze (compared to Sec. II) can be adopted where there is an overall scale factor in the metric. Such solutions can also exhibit the Hawking/Page phase transition on the gravity side, which can be used to probe confined/deconfined phase transition in dual two-dimensional QCD. Such solutions will be studied elsewhere in great detail.

which exist solely as the result of (well-known) primary hair such as gauge charges and hence are not really new characteristics, i.e., a primary hair endows a black hole with a new independent parameter (or the quantum number) whereas the secondary hair does not [79]. The charged dilaton black hole solutions [110,111] are examples of secondary hair, where nontrivial scalar field configuration is sourced by the electric charge (primary hair). The existence of secondary hair, therefore, does not really violate the no-hair theorem. In our work, the scalar hair is not sourced by the gauge field and can be continuously tuned to get the BTZ or charged BTZ solution in the limit $a \to 0$. It must also be stressed that the overwhelming majority of hairy black holes existing in literature usually possess a secondary hair, and solutions with primary hair are rare. See [109,112–114], for a few other cases where black hole solutions with primary hair were discussed.

The paper is structured as follows: In Sec. II, we discuss the three-dimensional Einstein-power Maxwell-scalar gravity model and present its analytic solution in terms of two functions $f(\phi)$ and $A(z)$. In Sec. III, we study the geometrical and thermodynamical properties of hairy black hole solution for the coupling $f(\phi) = 1$. In Secs. IV and V, we repeat the calculations with different couplings $f(\phi) = e^{\phi}$, and $f(\phi) = e^{\phi^2/2}$. In Sec. VI, we calculate the conserved mass of the black hole and establish the primary nature of the scalar hair. Finally, in Sec. VII, we conclude and summarize our results.

II. HAIRY CHARGED BLACK HOLE SOLUTION

To construct hairy-charged black holes with power Maxwell-like electrodynamics in three dimensions, we start with the following gravity action:

$$S = -\frac{1}{16\pi G_3}\int d^3x\sqrt{-g}\Big[R - \frac{1}{2}g^{\mu\nu}\partial_\mu\phi\partial_\nu\phi - V(\phi) + \frac{f(\phi)}{4}(s\mathcal{F})^{\frac{3}{4}}\Big], \tag{2.1}$$

where R denotes the Ricci scalar of the three-dimensional manifold $\mathcal{M}$, $V(\phi)$ is the potential of the scalar field ϕ, $f(\phi)$ corresponds to the coupling between the gauge and scalar fields, and $F_{\mu\nu}$ is the field strength tensor. In terms of the four-potential B_μ, $F_{\mu\nu}$ is expressed as $F_{\mu\nu} = \partial_\mu B_\nu - \partial_\nu B_\mu$. Note that, as discussed in the Introduction, the electromagnetic part of the action is traceless.

The variation of Eq. (2.1) gives the following Einstein, gauge, and scalar field equations:

$$R_{MN} - \frac{1}{2}g_{MN}R + \frac{1}{2}\left(\frac{g_{MN}}{2}\partial_P\phi\partial^P\phi - \partial_M\phi\partial_N\phi + g_{MN}V(\phi)\right) + \frac{f(\phi)}{4}(s\mathcal{F})^{-\frac{1}{4}}\left(-\frac{g_{MN}}{2}(s\mathcal{F}) + \frac{3}{2}(sF_{MP}F_N{}^P)\right) = 0, \tag{2.2}$$

$$\partial_\mu[\sqrt{-g}f(\phi)(s\mathcal{F})^{-\frac{1}{4}}F^{\mu\nu}] = 0, \tag{2.3}$$

$$\frac{1}{\sqrt{-g}}\partial_\mu[\sqrt{-g}\partial^\mu\phi] + \frac{1}{4}f'(\phi)(s\mathcal{F})^{\frac{3}{4}} = \frac{\partial V(\phi)}{\partial\phi}, \tag{2.4}$$

where $f'(\phi)$ denotes the derivative of the coupling function with respect to the field ϕ. We consider the following Ansaätze for the metric, scalar field, and gauge field to construct a static and spherically symmetric (S^1) hairy black hole solution in three dimensions:

$$ds^2 = \frac{L^2}{z^2}\left[-g(z)dt^2 + \frac{e^{2A(z)}dz^2}{g(z)} + d\theta^2\right], \qquad \phi = \phi(z), \qquad B_\mu = B_t(z)\delta^t_\mu, \tag{2.5}$$

where $A(z)$ is the form factor, whose form will be crucial in determining the hairy black hole solution and the corresponding thermodynamics, L is the AdS length scale, which we will set to one from here on for simplicity, and $g(z)$ is the blackening function. The radial coordinate z ranges from $z = 0$ (asymptotic boundary) to $z = z_h$ (black hole horizon radius) or to $z = \infty$ for thermal-AdS (without horizon).

There is only one nonzero component of Faraday's tensor in the geometry defined by (2.5), and that is $F_{tz} = -B_t'(z)$. So we can write $\mathcal{F} = 2F_{tz}^2 g^{tt}g^{zz} = 2B_t'^2(z)g^{tt}g^{zz}$. As a result, we set $s = -1$ to have real solutions for the gauge field while considering the electromagnetic Lagrangian's fractional power and maintaining generality. Now using Eq. (2.3), we get

$$F_{tz} = -B_t'(z) = -\frac{\sqrt{2}q_e e^{A(z)}}{f(\phi)^2}, \tag{2.6}$$

where q_e is an integration constant related to the charge of the black hole (see below). Similarly, by substituting (2.5) into (2.2), we get the following three Einstein equations of motion:

$$tt \equiv g'(z) - g(z)\left(\frac{2}{z} + 2A'(z) + \frac{1}{2}z\phi'(z)^2\right) - \frac{V(\phi)e^{2A(z)}}{z} - \frac{f(\phi)e^{2A(z)}(s\mathcal{F})^{\frac{3}{4}}}{8z} = 0, \tag{2.7}$$

$$zz \equiv g'(z) - g(z)\left(\frac{2}{z} - \frac{1}{2}z\phi'(z)^2\right) - \frac{V(\phi)e^{2A(z)}}{z} - \frac{f(\phi)e^{2A(z)}(s\mathcal{F})^{\frac{3}{4}}}{8z} = 0, \tag{2.8}$$

$$\theta\theta \equiv g''(z) - g'(z)\left(\frac{2}{z} + A'(z)\right) + g(z)\left(\frac{2}{z^2} + \frac{2A'(z)}{z} + \frac{1}{2}\phi'(z)^2\right) + \frac{V(\phi)e^{2A(z)}}{z^2} - \frac{f(\phi)e^{2A(z)}(s\mathcal{F})^{\frac{3}{4}}}{4z^2} = 0. \tag{2.9}$$

The above three equations can be further rearranged into the following equations:

$$g''(z) - g'(z)\left(\frac{1}{z} + A'(z)\right) - \frac{3f(\phi)e^{2A(z)}(s\mathcal{F})^{\frac{3}{4}}}{8z^2} = 0, \tag{2.10}$$

$$\frac{\phi'(z)^2}{2} + \frac{A'(z)}{z} = 0, \tag{2.11}$$

$$g''(z) - g'(z)\left(\frac{3}{z} + A'(z)\right) + g(z)\left(\frac{4}{z^2} + \frac{2A'(z)}{z}\right)\frac{2V(\phi)e^{2A(z)}}{z^2} - \frac{f(\phi)e^{2A(z)}(s\mathcal{F})^{\frac{3}{4}}}{8z^2} = 0. \tag{2.12}$$

Similarly, the scalar field equation of motion is given by

$$\phi''(z) - \phi'(z)\left(A'(z) - \frac{g'(z)}{g(z)} + \frac{1}{z}\right) - \frac{e^{2A(z)}}{z^2 g(z)}\frac{\partial V(\phi)}{\partial \phi} - \frac{e^{2A(z)}(s\mathcal{F})^{3/4}}{4z^2 g(z)}\frac{\partial f(\phi)}{\partial \phi} = 0. \tag{2.13}$$

Therefore, overall, we have five equations of motion in the gravity system of Eq. (2.1). However, only four of them are independent. It can be explicitly checked that the last Eq. (2.13) follows from the Bianchi identity and is therefore redundant. Below we will choose Eq. (2.13) as a constrained equation and consider the rest of the equations as independent. We now impose the following boundary conditions to solve these equations:

$$\begin{aligned} &g(0) = 1, \quad \text{and} \quad g(z_h) = 0, \\ &B_t(0) = \mu_e, \quad \text{and} \quad B_t(z_h) = 0, \\ &A(0) = 0. \end{aligned} \tag{2.14}$$

The boundary conditions at $z = 0$ are chosen to ensure that the spacetime asymptotes to AdS at the boundary. The parameter μ_e is the leading term of the near boundary expansion of the gauge field $B_t(z)$ and corresponds to the chemical potential of the theory. Using Gauss's theorem, we can also find a relation between μ_e and the electric charge of the black hole (see the discussion below). In addition to these boundary conditions, we further require that the scalar field goes to zero at the boundary $\phi(0) = 0$ and must remain real throughout the bulk.

Using the above boundary conditions and solving Eq. (2.6), we get the following solution for the gauge field:

$$B_t(z) = \sqrt{2}q_e \int_z^{z_h} d\xi \frac{e^{A(\xi)}}{f^2(\xi)}. \tag{2.15}$$

Similarly, by solving Eq. (2.10), the solution for $g(z)$ is

$$g(z) = C_1 + \int_0^z d\xi e^{A(\xi)}\xi[C_2 + \mathcal{K}(\xi)], \tag{2.16}$$

where

$$\mathcal{K}(\xi) = \frac{3q_e^{3/2}}{2\sqrt{2}} \int d\xi \frac{e^{A(\xi)}}{f^2(\xi)}, \tag{2.17}$$

where the integration constants C_1 and C_2 are

$$C_1 = 1, \qquad C_2 = -\frac{1 + \int_0^{z_h} d\xi e^{A(\xi)}\xi\mathcal{K}(\xi)}{\int_0^{z_h} d\xi e^{A(\xi)}\xi}. \tag{2.18}$$

The expression of scalar field ϕ can be similarly found by solving Eq. (2.11):

$$\phi(z) = \int dz \sqrt{\frac{-2A'(z)}{z}} + C_3, \tag{2.19}$$

where C_3 can be obtained by demanding ϕ to vanish near the asymptotic boundary, i.e., $\phi|_{z=0} \to 0$. Lastly, the potential V can be found from Eq. (2.12),

$$V(z)=\frac{1}{16}e^{-2A(z)}(8z^2A'(z)+24z)g'(z)+\frac{1}{16}e^{-2A(z)}g(z)(-16zA'(z)-32)+\frac{z^3f(z)(e^{-2A(z)}B_t'(z)^2)^{3/4}}{8\sqrt[4]{2}}-\frac{1}{2}z^2e^{-2A(z)}g''(z). \tag{2.20}$$

It is thus clear that Eqs. (2.15)–(2.20) exhibit a closed-form analytic solution of the gravity system of Eq. (2.1) in $(2+1)$-dimensions in terms of two functions $A(z)$ and $f(z)$. The constructed hairy solution will depend only on $A(z)$ once the coupling function $f(\phi)$ is fixed. However, different forms of $A(z)$ and $f(\phi)$ will correspond to different $V(z)$, i.e., various $A(z)$ and $f(\phi)$ will ascribe to different $(2+1)$-dimensional hairy black hole solutions. Therefore, by selecting different forms of $A(z)$ and $f(\phi)$, one may systematically construct a vast family of physically permissible primary hair charged black hole solutions for the Einstein-power Maxwell-scalar gravity system in $(2+1)$ dimensions.

In the context of applied gauge/gravity duality, the forms of $A(z)$ and $f(\phi)$ are often determined or fixed by demanding a sensible dual boundary field theory. In particular, suitable forms of $A(z)$ and $f(\phi)$ are typically taken depending on the sort of boundary field theory one is interested in. For instance, in the field of holographic QCD, the forms of these functions are typically fixed by requiring the dual boundary field theory to exhibit genuine QCD characteristics, such as confinement/deconfinement phase transition [115–117], confinement in the quark sector, linear Regge trajectory for the excited meson mass spectrum, etc. In such model-building cases, the form $A(z)=-a^2z^2$ is generally considered [94,101,103].

However, we can also take a more liberal and phenomenological approach and investigate various physically motivated forms of $A(z)$ and $f(\phi)$ to thoroughly discuss the effects of scalar hair and make qualitative arguments about the stability and thermodynamics of the hairy-charged black holes in three dimensions with Maxwell-like electrodynamics, without worrying too much about the dual boundary field theory. Here, we take such an approach. In particular, we take three physically motivated forms of the coupling function: (i) $f(\phi)=1$; (ii) $f(\phi)=e^{\phi}$; and (iii) $f(\phi)=e^{\phi^2/2}$. As mentioned earlier, these three types of couplings have recently received a lot of attention in several contexts involving hairy black holes; for example, see [107]. It is, therefore, interesting to examine how these coupling functions influence the hairy black hole structure in three dimensions as well. Similarly, following [96], we focus on a particularly straightforward form of $A(z)=-a^2z^2$. In addition to being simpler, this form of $A(z)$ is particularly chosen as it gives us more control over the integrals that show up in the solutions of various geometric functions discussed above. This form of $A(z)$ has also been widely employed in the holographic QCD literature; for instance, see [94,101]. With the considered form of $A(z)=-a^2z^2$, the parameter a determines the strength and backreaction of the scalar field. As a result, the scalar field backreaction drops to zero when the parameter a goes to zero. Thus, as desired, one returns to the charged BTZ black-hole-like solution with Maxwell-like electrodynamics in the limit $a\to 0$.

There are also other important reasons for taking the above-mentioned forms of $f(\phi)$ and $A(z)$:

(1) They ensure that the obtained hairy solution asymptotes to AdS, i.e., at the boundary $z\to 0$, we have

$$V(z)|_{z\to 0}=-\frac{2}{L^2}+\frac{m^2\phi^2}{2}+\ldots,$$
$$V(z)|_{z\to 0}=2\Lambda+\frac{m^2\phi^2}{2}+\ldots, \tag{2.21}$$

where, as usual, $\Lambda=-\frac{1}{L^2}$ is the negative cosmological constant in three dimensions. Similarly, the Ricci scalar R approaches $-6/L^2$ asymptotically. This, together with the fact that $g(z)|_{z\to 0}=1$, indeed ensures that the obtained solutions asymptote to AdS at the boundary. Moreover, the mass of the scalar field $m^2=-1$ also satisfies the Breitenlohner-Freedman bound for stability in AdS space, i.e., $m^2\geq -1$ [118].

(2) Furthermore, as we will show shortly, the hairy solutions satisfy the Gubser criterion to have a well-defined dual boundary field theory [108].

(3) These forms of $f(z)$ and $A(z)$ also ensure that the null energy condition is always respected in our gravity model. The null energy condition can be expressed as

$$T_{MN}\mathcal{N}^M\mathcal{N}^N\geq 0, \tag{2.22}$$

where the null vector $\mathcal{N}^M$ satisfies the condition $g_{MN}\mathcal{N}^M\mathcal{N}^N=0$ and T_{MN} is the energy-momentum tensor of the matter fields. The null vector $\mathcal{N}^M$ can be chosen as

$$\mathcal{N}^M=\frac{1}{\sqrt{g(z)}}\mathcal{N}^t+\frac{\cos\alpha\sqrt{g(z)}}{e^{A(z)}}\mathcal{N}^z+\sin\alpha\mathcal{N}^\theta, \tag{2.23}$$

for arbitrary parameter α. The null energy condition then becomes

$$T_{MN}\mathcal{N}^M\mathcal{N}^N = \frac{3zf(z)\sin^2\alpha(e^{-2A(z)}B_t'(z)^2)^{3/4}}{8\sqrt[4]{2}} + \frac{1}{2}e^{-2A(z)}g(z)\cos^2\alpha\phi'(z)^2 \geq 0, \tag{2.24}$$

which is always satisfied everywhere outside the horizon for the chosen forms of $A(z)$ and $f(\phi)$.

Now that the hairy black hole solutions have been constructed, let us write down the expressions for various thermodynamic quantities. This will be useful later in discussing hairy black hole thermodynamics. The black hole temperature (T) and entropy ($S_{\rm BH}$) are given by

$$T = -\frac{e^{-A(z_h)}g'(z_h)}{4\pi}, \qquad S_{\rm BH} = \frac{\mathcal{A}}{4G_3} = \frac{2\pi}{4G_3 z_h}, \tag{2.25}$$

where $\mathcal{A} = 2\pi/z_h$ is the area of the event horizon. Similarly, we can compute the electric charge Q of the black hole by measuring the flux of the electric field at the boundary,

$$Q_e = \frac{3}{16\pi G_3}\int \frac{f(\phi)}{4}(s\mathcal{F})^{-\frac{1}{4}}F_{\mu\nu}u^\mu n^\nu d\theta, \tag{2.26}$$

where u^μ and n^ν are the unit spacelike and timelike normals to the constant radial surface, respectively,

$$u^\mu = \frac{1}{\sqrt{-g_{tt}}}\delta_t^\mu = \frac{z}{L\sqrt{g(z)}}\delta_t^\mu, \qquad n^\nu = \frac{1}{\sqrt{g_{zz}}}\delta_z^\nu = \frac{z\sqrt{g(z)}}{Le^{A(z)}}\delta_z^\nu, \tag{2.27}$$

and $d\theta$ represents the integration across the one-dimensional boundary space. Using (2.6), and after simplification, we obtain the following expression of the black hole charge:

$$Q_e = \frac{3\sqrt{q_e}}{64\pi G_3}. \tag{2.28}$$

We can also find a relation between the electric charge and the corresponding conjugate chemical potential μ_e. The chemical potential is the leading term of the near boundary expansion of the gauge field $B_t(z)$. Substituting $B_t(z)$ from Eq. (2.15) into Eq. (2.6), we get

$$\mu_e = \sqrt{2}q_e\int_0^{z_h} d\xi \frac{e^{A(\xi)}}{f^2(\xi)}. \tag{2.29}$$

With hairy black hole solution in hand, let us also mention that there exists another solution to the gravity equations of motion. This solution does not exhibit the horizon and is called thermal AdS.[3] The thermal-AdS solution can be derived from the black hole solution by taking the limit $z_h \to \infty$. Depending on the nature of $A(z)$, the thermal AdS may have a nontrivial structure in the bulk. However, due to the imposed boundary conditions (2.14), and just like in the case of black hole solution, it always asymptotes to AdS at the boundary. Intriguingly, as we shall show later, depending on the magnitudes of a and $\{\mu_e, q_e\}$, there may also be a Hawking/Page type thermal-AdS/black hole phase transition between these two solutions.

III. HAIRY BLACK HOLE SOLUTION WITH COUPLING $f(\phi) = 1$

In this section, we will first look at the geometric and thermodynamic properties of the hairy black hole solution for the simplest coupling function $f(\phi) = 1$. With the considered form factor $A(z) = -a^2z^2$, the solution for the scalar field is

$$\phi(z) = 2az. \tag{3.1}$$

From the Eq. (2.6), we have $F_{tz} = -\sqrt{2}q_e e^{-a^2z^2}$. This gives us the gauge field solution

$$B_t(z) = \frac{\sqrt{\pi}q_e(\mathrm{erf}(az_h) - \mathrm{erf}(az))}{\sqrt{2}a}, \tag{3.2}$$

where erf is the error function. Notice that the scalar field vanishes in the limit $a \to 0$. Similarly, in the limit $a \to 0$, the gauge field also reduces to

$$B_t(z) = \sqrt{2}q_e(z_h - z), \tag{3.3}$$

indicating that the electrodynamics employed here in three dimensions for a nonhairy black hole is Maxwellian type. Using Eq. (2.29), we can further find the relation between μ_e and q_e:

$$q_e = \sqrt{\frac{2}{\pi}}\frac{a\mu_e}{\mathrm{erf}(az_h)}. \tag{3.4}$$

Now, Using the Eq. (2.10), we have the following solution for $g(z)$:

[3]We will refer to this without horizon solution as thermal AdS here for convenience, even though this solution does not have a constant curvature throughout the spacetime.

$$g(z) = \frac{1 - e^{a^2(z_h^2 - z^2)}}{1 - e^{a^2 z_h^2}} + \frac{3\sqrt{\pi} e^{-a^2 z^2} q_e^{3/2} (e^{a^2 z^2} \mathrm{erf}(\sqrt{2} a z) - \sqrt{2}\mathrm{erf}(a z))}{16 a^3} + \frac{3\sqrt{\pi} e^{-a^2 z^2} (e^{a^2 z^2} - 1) q_e^{3/2} (\sqrt{2}\mathrm{erf}(a z_h) - e^{a^2 z_h^2} \mathrm{erf}(\sqrt{2} a z_h))}{16 a^3 (e^{a^2 z_h^2} - 1)}. \tag{3.5}$$

Note that in the limit $a \to 0$, this expression reduces to the charged black hole expression found in [26] with a Maxwell-like potential, i.e.,

$$g(z) = 1 - \frac{z^2}{z_h^2} - \frac{z^2 z_h q_e^{3/2}}{2\sqrt{2}} + \frac{z^3 q_e^{3/2}}{2\sqrt{2}}. \tag{3.6}$$

Similarly, we have calculated $V(z)$, but since it is rather long and not very informative, we prefer not to write it down here for brevity.

In Fig. 1, the radial profile of $g(z)$, Kretschmann scalar $R_{\mu\nu\rho\sigma}R^{\mu\nu\rho\sigma}$, scalar field, and the potential is shown for different values of scalar hair parameter a. Note that, at $z = z_h$, $g(z)$ changes its sign, indicating the presence of a horizon. This is true for all values of a. Similarly, the Ricci and Kretschmann scalars are finite everywhere outside the horizon. The curvature singularity appears only at $z = 1/r = \infty$, which is shielded by the horizon. Therefore, there is no additional singularity in the hairy black hole case than those already present at the nonhairy-charged BTZ black hole. Note that in the usual three-dimensional Einstein-Maxwell gravity system, the curvature is constant throughout the spacetime for the uncharged BTZ case. The curvature singularity arises only when the charge is added. The same is true for the Einstein-power Maxwell gravity system. However, in the presence of scalar hair, the curvature singularity can arise even when the charge is zero, i.e., the strength of the singularity increases with the scalar hair. In particular, $R_{\mu\nu\rho\sigma}R^{\mu\nu\rho\sigma} \propto z^2$ for the charged BTZ case, whereas $R_{\mu\nu\rho\sigma}R^{\mu\nu\rho\sigma} \propto z^6$ for the hairy case of fractional power law electrodynamics employed here. This can be clearly observed in Fig. 1(b). Interestingly, compared to the Einstein-Maxwell-scalar gravity system, where there is an additional logarithmic singularity at the center of the black hole ($R_{\mu\nu\rho\sigma}R^{\mu\nu\rho\sigma} \propto z^6 \log z$) [88], the strength of the singularity is milder in the case of Einstein-power Maxwell-scalar gravity system where no such logarithmic singularity arises. This is expected considering that the gauge field gives $\log z$

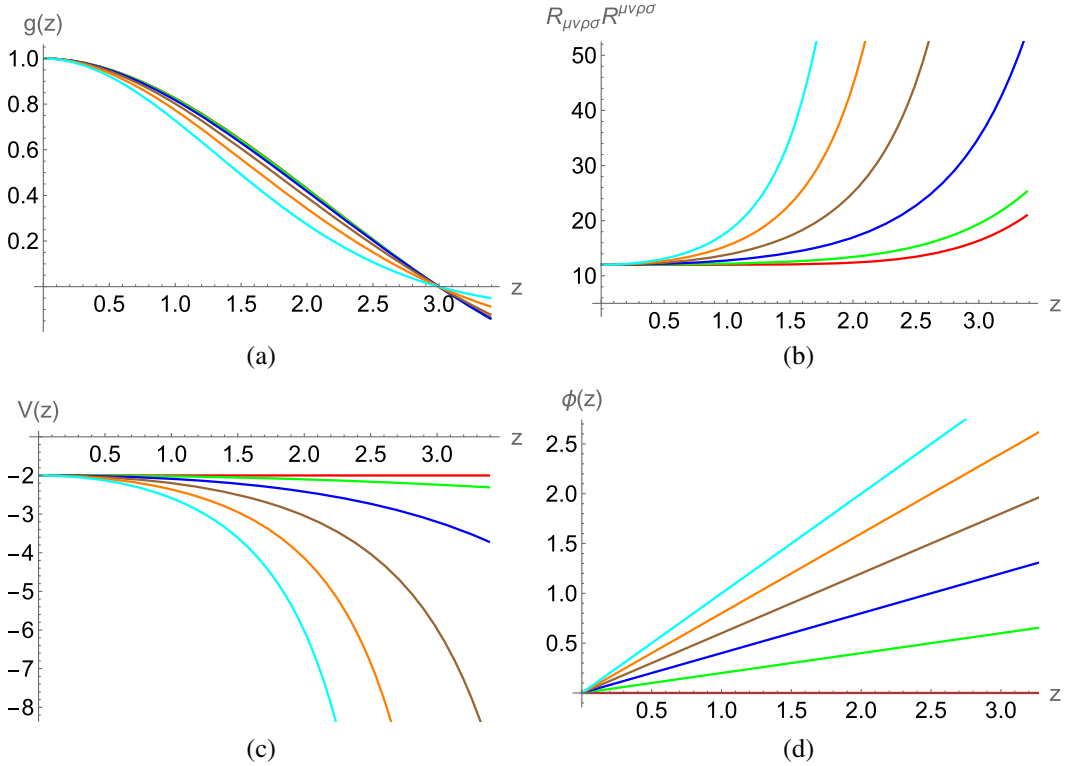

FIG. 1. The nature of $g(z)$, $R_{\mu\nu\rho\sigma}R^{\mu\nu\rho\sigma}$, $\phi(z)$, and $V(z)$ for different values of hairy parameter a. Here $z_h = 3.0$ and $q_e = 0.15$ are used. Red, green, blue, brown, orange, and cyan curves correspond to $a = 0, 0.1, 0.2, 0.3, 0.4$, and 0.5, respectively.

contribution to $g(z)$, thereby giving additional $\log z$ contributions to the curvature scalars in the Einstein-Maxwell theory, whereas no such contribution arises in the Einstein-power Maxwell theory.

Also, the scalar field is finite and real everywhere at and outside the horizon and only goes to zero at the asymptotic boundary. This suggests the presence of a well-behaved hairy black hole solution with Maxwell-like electrodynamics in three dimensions. In the outer horizon area, the potential is similarly regular and limited. The potential asymptotes to $V(z=0)=-2/L^2$ at the boundary for all a and q_e. Moreover, provided that the charge q_e is not too large, the potential is also bounded from above by its UV boundary value, i.e., $V(0)\geq V(z)$, hence satisfying the Gubser criterion to have a well-defined boundary field theory [108]. However, the said criterion can be violated for higher values of $q_e \gtrsim 5$. In the rest of the work, we will concentrate on only those parameter values for which the Gubser criterion is respected.

Now, let us discuss the thermodynamics of the black hole. For $f(\phi)=1$, the expression of the black hole temperature is given by

$$T=\frac{a^2 z_h e^{a^2 z_h^2}}{2\pi(e^{a^2 z_h^2}-1)} + \frac{q_e^{3/2} z_h e^{a^2 z_h^2}(3\sqrt{\pi}\,\mathrm{erf}(\sqrt{2}a z_h)-3\sqrt{2\pi}\,\mathrm{erf}(a z_h))}{32\pi a(e^{a^2 z_h^2}-1)}. \tag{3.7}$$

The aforementioned expression smoothly reduces to the typical charged BTZ-like expression in the limit when $a\to 0$, i.e.,

$$T|_{a\to 0}=\frac{1}{2\pi z_h}-\frac{q_e^{3/2} z_h^2}{8\sqrt{2}\pi}, \tag{3.8}$$

which also indicates that the black hole can become extremal when the charge is added to the system, as opposed to the uncharged case.

Let us first discuss the black hole thermodynamics in the grand-canonical ensemble. Figure 2 illustrates the temperature variation with regard to the (inverse) horizon radius z_h for various values of hairy parameter a. Here we have kept $\mu_e=0$ fixed, which is also equivalent to $q_e=0$. Observe that for $a=0$ (red line), there is only one black hole phase. The temperature of this phase decreases with z_h and has a positive specific heat. Correspondingly, this black hole phase is thermodynamically stable. The local thermodynamic stability of the hairy black holes will be discussed shortly. This is an expected result considering that for $a=0$ and $\mu_e=0$, our hairy solution reduces to the stable uncharged BTZ black hole, which is thermodynamically stable at all temperatures.

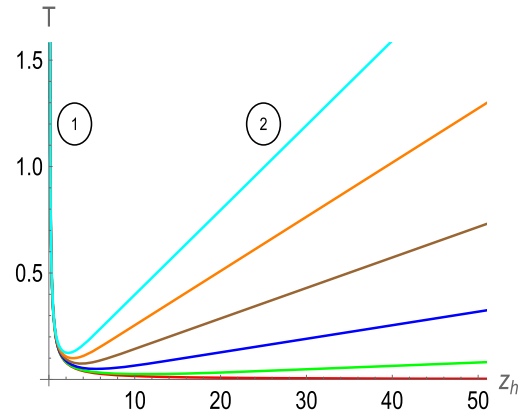

FIG. 2. Hawking temperature T as a function of horizon radius z_h for various values of a. Here $\mu_e=0$ is used. Red, green, blue, brown, orange, and cyan curves correspond to $a=0, 0.1, 0.2, 0.3, 0.4$, and 0.5, respectively.

The thermodynamic structure changes drastically when the hairy parameter a is switched on. With finite a, there are now two black hole phases at a fixed temperature: a small phase (unstable) and a large phase (stable). These stable and unstable phases are marked by ① and ②, respectively, in Fig. 2. While the temperature increases with z_h for the small-unstable black hole phase, it falls with z_h for the large-stable black hole phase (cyan line). The appearance of the small-unstable phase can also be analytically noticed from Eq. (3.7). Observe that for $\mu_e=0$, the second term vanishes, and only the first term contributes to the temperature, and this first term increases with z_h for large z_h. Interestingly, unlike the uncharged BTZ black hole, the uncharged hairy black hole phases exist only above a certain minimum temperature $T_{\min}$, i.e., below $T_{\min}$, the hairy black hole phases cease to exist and leaving the thermal-AdS solution as the only remaining feasible phase. This is true for all finite values of a. Importantly, as it generally happens, the occurrence of multivaluedness of the temperature also indicates a possible phase transition in the hairy context.

To further investigate the global thermodynamic stabilities of the above-discussed hairy black hole phases, we need to study their free energy behavior. The Gibbs free energy $\mathcal{G}$ at a fixed potential in differential form is related to the black hole entropy as

$$d\mathcal{G}=-S_{\mathrm{BH}}dT, \tag{3.9}$$

which can be used to compute the free energy difference between the black hole and thermal-AdS phases,

$$\Delta\mathcal{G}=-\int S_{\mathrm{BH}}dT=-\int_{z_\Lambda=\infty}^{z_h} S_{\mathrm{BH}}\frac{dT}{dz_h}dz_h. \tag{3.10}$$

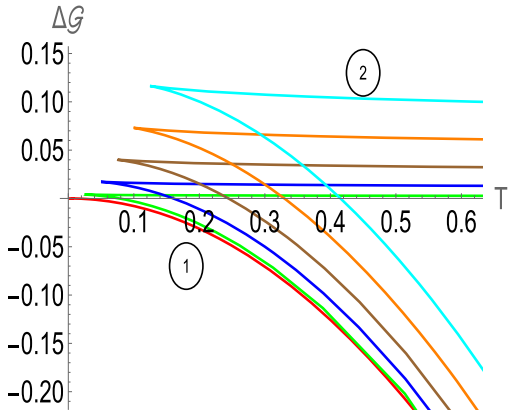

FIG. 3. The Gibbs free energy difference $\Delta\mathcal{G}$ as a function of T for various values of a. Here $\mu_e = 0$ is used. Red, green, blue, brown, orange, and cyan curves correspond to $a = 0, 0.1, 0.2, 0.3, 0.4$, and 0.5, respectively.

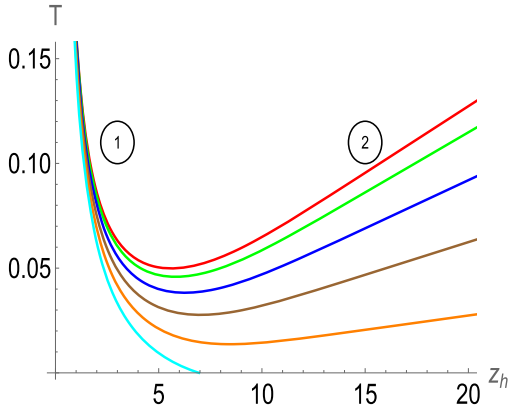

FIG. 4. Hawking temperature T as a function of horizon radius z_h for various values of chemical potential μ_e. Here, $a = 0.2$ is used. Red, green, blue, brown, orange, and cyan curves correspond to $\mu_e = 0, 0.2, 0.4, 0.6, 0.8$, and 1.0, respectively.

In Fig. 3, the Gibbs free energy of the hairy black hole phases is shown.[4] The color pattern used here is identical to Fig. 2. We observe that for all finite values of a, there appears a transition temperature $T_{\rm HP}$ at which the Gibbs free energy changes its sign. It suggests the occurrence of a well-known Hawking/Page type phase transition between an uncharged large-stable hairy black hole phase and the thermal-AdS phase at $T_{\rm HP}$. Accordingly, below $T_{\rm HP}$ thermal AdS is thermodynamically favored, whereas above $T_{\rm HP}$ large hairy black hole is thermodynamically favored. Also, the free energy of the small-unstable black hole phase is always higher than the large-stable black hole phase, indicating that the small-unstable black hole phase is always thermodynamically disfavored for the large-stable black hole phase.

The above thermodynamic structure of the hairy black hole gets more interesting as the chemical potential is turned on. Depending upon the relative magnitudes of μ_e and a, not only the hairy black hole can become extremal, but it can also exist in one or two phases. This is illustrated in Fig. 4. Here, we have presented the results for a particular value of $a = 0.2$; however, analogous results appear for other values of a as well. For small μ_e, like in the $\mu_e = 0$ case, there again appear two black hole phases above $T_{\rm min}$, with the large black hole phase (indicated by ①) being thermodynamically more favored and stable compared to the small black hole phase (indicated by ②) at all temperatures $T > T_{\rm min}$. Therefore, for small μ_e, there again occurs a Hawking/Page phase transition between the large hairy black hole and thermal-AdS phases. This is illustrated in Fig. 5, where one can clearly observe a sign change in the Gibbs free energy as the temperature is varied. However, for large μ_e, this phase transition ceases to exit. For large μ_e, there exists only one stable black hole phase which becomes extremal at some horizon radius $z_h^{\rm ext}$ (cyan line), and the free energy of this black hole phase is always smaller than the thermal AdS. This result is completely analogous to the charged BTZ black hole. For the nonhairy-charged BTZ black hole (with Coulomb-like potential), the extremal horizon radius can be found from Eq. (3.8). It occurs at $z_h^{\rm ext} = 4(2)^{1/6}/\mu_e$, whereas for the hairy black hole case, the magnitude of this $z_h^{\rm ext}$ increases with a. These results further imply that irrespective of the temperature, at least one black hole phase always exists and remains stable for the charged case when μ_e is relatively large. Our whole analysis, therefore, suggests that for a fixed value of a, there exists a critical chemical potential μ_e^c below which the Hawking/Page phase transition between the thermal-AdS and hairy black hole phases takes place, whereas no such phase transition appears above μ_e^c.

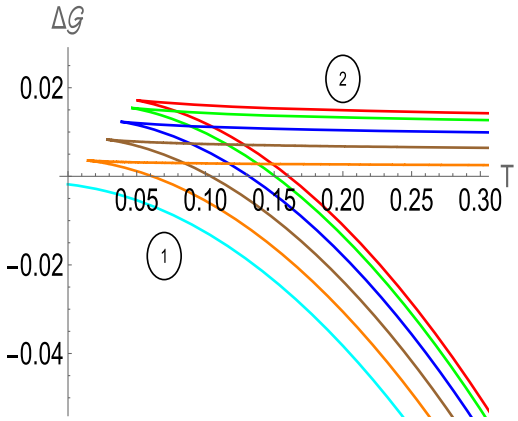

FIG. 5. The Gibbs free energy difference $\Delta\mathcal{G}$ as a function of T for various values of chemical potential μ_e. Here $a = 0.2$ is used. Red, green, blue, brown, orange, and cyan curves correspond to $\mu_e = 0, 0.2, 0.4, 0.6, 0.8$, and 1.0, respectively.

[4]Here, we have taken the upper limit of integration $z_\Lambda = 10^6$ in the numerical computation.

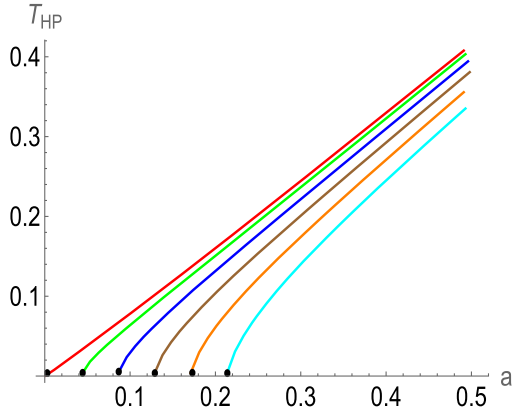

FIG. 6. Hawking/Page phase transition temperature T_{HP} as a function of a for various values of chemical potential μ_e. Red, green, blue, brown, orange, and cyan curves correspond to $\mu_e = 0, 0.2, 0.4, 0.6, 0.8,$ and 1, respectively. The black dots indicate the critical hairy parameter a_c.

We further investigate the dependence of T_{HP} on a and μ_e. Figures 6 and 7 depict the overall dependence of T_{HP} on these variables. Our finding shows that when a increases, T_{HP} shows a monotonically rising tendency. Specifically, the transition temperature rises with a while falling with μ_e. Although T_{HP} rises with a for every μ_e, it should be noted that, unlike the $\mu_e = 0$ case, the slope of the a vs T_{HP} line is not constant for finite μ_e. Our results, therefore, suggest that the possibility of Hawking/Page phase transition in the hairy context increases for large a and small μ_e values. It also implies that for large chemical potential, one needs a higher value of a to observe the Hawking/Page phase transition. This, in turn, implies the existence of critical hairy parameter a_c below which no Hawking/Page phase transition takes place in the fixed μ_e grand-canonical ensemble.

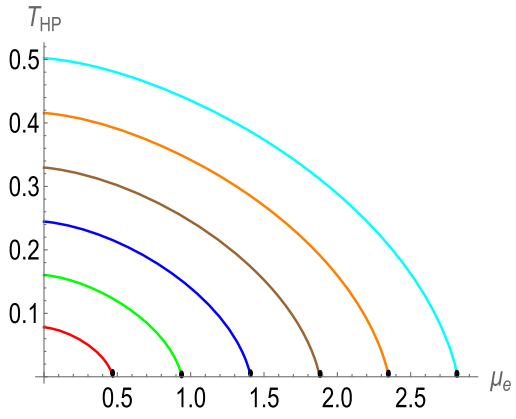

FIG. 7. Hawking/Page phase transition temperature T_{HP} as a function of chemical potential μ_e for various values of a. Red, green, blue, brown, orange, and cyan curves correspond to $a = 0.1, 0.2, 0.3, 0.4, 0.5,$ and 0.6, respectively. The black dots indicate the critical chemical potential μ_e^c.

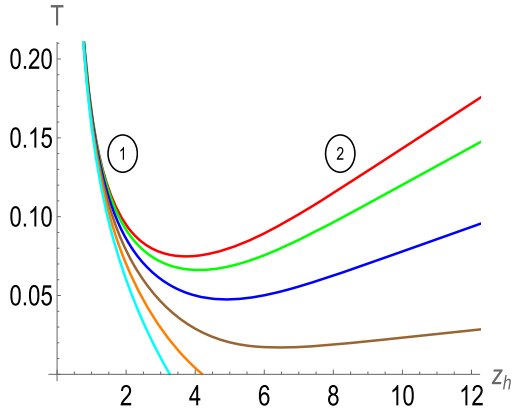

FIG. 8. Hawking temperature T as a function of horizon radius z_h for various values of charge q_e. Here, $a = 0.3$ is used. Red, green, blue, brown, orange, and cyan curves correspond to $q_e = 0, 0.1, 0.2, 0.3, 0.4,$ and 0.5, respectively.

Having discussed the thermodynamic structure of the hairy black hole in the grand-canonical ensemble, we now move on to discuss it in the canonical ensemble. We find that the thermodynamic results in the canonical ensemble are quite similar to the grand-canonical ensemble. The case $q_e = 0 = \mu_e$ is already discussed above. The results for finite q_e are shown in Figs. 8 and 9. In the canonical ensemble as well, depending upon the magnitude of a, there appear two black hole phases for small q_e, whereas only one black hole phase appears for large q_e. While the temperature increases with z_h for the unstable black hole phase, it falls with z_h for the stable black hole phase. The temperature expression shows that for $q_e \neq 0$ and very small values of a, there is only one stable branch of the black hole, and it becomes extremal at some horizon radius z_h^{ext} (orange and cyan lines). These findings also suggest that, for the fixed charged case, at least one stable black hole branch always exists when a is relatively small. While keeping q_e fixed, the temperature starts to rise with z_h for

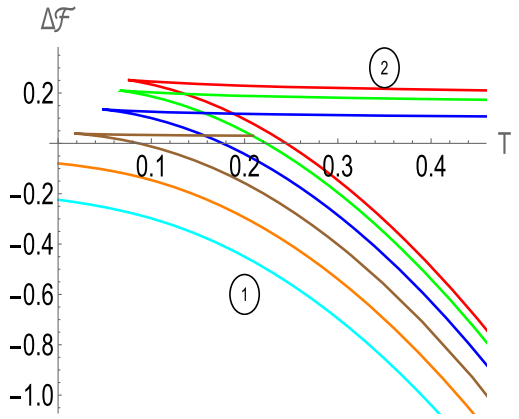

FIG. 9. The Helmholtz free energy difference $\Delta\mathcal{F}$ as a function of T for various values of charge q_e. Here $a = 0.3$ is used. Red, green, blue, brown, orange, and cyan curves correspond to $q_e = 0, 0.1, 0.2, 0.3, 0.4,$ and 0.5, respectively.

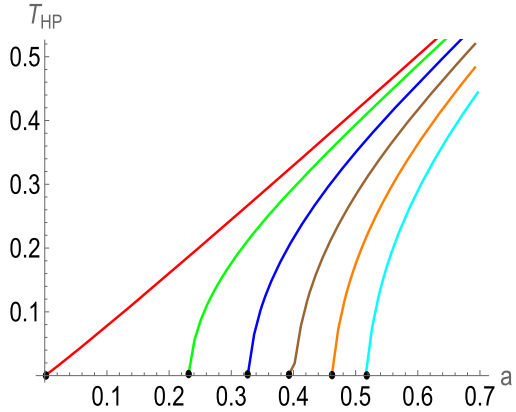

FIG. 10. Hawking/Page phase transition temperature $T_{\rm HP}$ as a function of a for various values of q_e. Red, green, blue, brown, orange, and cyan curves correspond to $q_e = 0, 0.2, 0.4, 0.6, 0.8$, and 1.0, respectively. The black dots indicate the critical hairy parameter a_c.

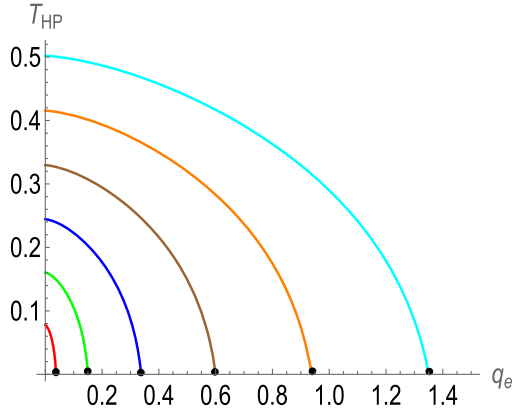

FIG. 11. Hawking/Page phase transition temperature $T_{\rm HP}$ as a function of q_e for various values of a. Red, green, blue, brown, orange, and cyan curves correspond to $a = 0.1, 0.2, 0.3, 0.4, 0.5$, and 0.6, respectively. The black dots indicate the critical charge q_e^c.

large a values. Notably, the hairy black hole phases are restricted to temperatures over a certain threshold $T_{\rm min}$, in contrast to the BTZ black hole. This suggests the possibility of Hawking/Page transition between large hairy black hole phase and thermal AdS as a increases in the canonical ensemble as well. This is indeed the case, as can be explicitly observed from the free energy behavior shown in Fig. 9. The Helmholtz free energy difference between the black hole and thermal-AdS phases can be computed from the analogous differential first law,

$$d\mathcal{F} = -S_{\rm BH} dT,$$
$$\Delta\mathcal{F} = \int_{z_h}^{z_\Lambda=\infty} S_{\rm BH} \frac{dT}{dz_h} dz_h. \tag{3.11}$$

The transition temperature $T_{\rm HP}$ again depends nontrivially on a and q_e. Figures 10 and 11 show the full illustration of this dependency. Our analysis shows that when a changes, $T_{\rm HP}$ shows a monotonically rising tendency. Specifically, the transition temperature rises with a while falling with q_e. Although $T_{\rm HP}$ rises with a for every q_e, it should be noted that, unlike the situation where $q_e = 0$, the slope of the a vs $T_{\rm HP}$ line is not constant for $q_e \neq 0$. Overall, our analysis suggests that there exists a critical value a_c of the hairy parameter in the fixed charge ensemble as well. The charged hairy black hole undergoes the Hawking/Page phase transition above this critical value, while below a_c, no such phase transition takes place.[5]

[5]Here we like to emphasize that the Helmholtz free energy difference cannot be computed from Eq. (3.11) for nonhairy black holes corresponding to $a \to 0$. This is because the integrand in Eq. (3.11) contains z_h^3 and $\log z_h$ terms which give diverging contributions to the free energy difference in the upper limit of integration. For this reason, here as well as in the subsequent sections, we discuss thermodynamic results only for the hairy case in the canonical ensemble.

Let us emphasize that the obtained hairy black holes are also locally stable. The local stability corresponds to the response of the equilibrium system under a small fluctuation in thermodynamical variables and is established by the positivity of the specific heat at a constant chemical potential $C_{\mu_e} = T(\partial S_{\rm BH}/\partial T)|_{\mu_e}$ or charge $C_{q_e} = T(\partial S_{\rm BH}/\partial T)|_{q_e}$ in the grand-canonical and canonical ensembles, respectively. Since $S_{\rm BH} \propto z_h^{-1}$, it is straightforward to see from Figs. 2 and 8 that the slope of the $S_{\rm BH} - T$ plane is always positive in the thermodynamically favored hairy black hole phase ①. Accordingly, $C_{\mu_e} > 0$ and $C_{q_e} > 0$ in the favored hairy black hole phase, indicating the local stability of hairy black holes. Similarly, C_{μ_e} and C_{q_e} are negative in the thermodynamically disfavored hairy black hole phase ②.

IV. HAIRY BLACK HOLE SOLUTION WITH COUPLING $f(\phi) = e^{\phi}$

In this section, we investigate the geometrical and thermodynamical structure of the charged hairy black hole solutions for the exponential coupling function $f(\phi) = e^{\phi}$. The form of $A(z) = -a^2 z^2$ is the same as in the previous section. Therefore, the solution of the scalar field will remain the same. This indicates that the scalar field remains regular, finite, and well behaved everywhere outside the horizon for this coupling as well. From the Eq. (2.6), we get the gauge field solution

$$B_t(z) = \frac{q_e \sqrt{\pi} e^4}{\sqrt{2} a} (\mathrm{erf}(2 + a z_h) - \mathrm{erf}(2 + a z)), \tag{4.1}$$

with relation between μ_e and q_e as

$$q_e = \sqrt{\frac{2}{\pi}} \frac{a \mu_e}{e^4 (\mathrm{erf}(2 + a z_h) - \mathrm{erf}(2))}. \tag{4.2}$$

Notice that in the limit $a \to 0$, $B_t(z)$ again reduces to the Coulomb-like potential. In a similar manner, we obtain the following expression for $g(z)$:

$$g(z) = \frac{1-e^{a^2(z_h^2-z^2)}}{1-e^{a^2 z_h^2}} + \frac{3\sqrt{\pi}q_e^{3/2}(\sqrt{2}e^2\mathrm{erf}(2)-\mathrm{erf}(\sqrt{2}))e^{2-a^2z^2}(e^{a^2z_h^2-e^{a^2z^2}})}{16a^3(e^{a^2z_h^2}-1)} + \frac{3q_e^{3/2}\sqrt{\pi}e^{4-a^2z^2}(e^{a^2z^2}-1)\mathrm{erf}(2+az_h)}{8\sqrt{2}a^3(e^{a^2z_h^2}-1)} + \frac{3e^2\sqrt{\pi}q_e^{3/2}\mathrm{erf}(\sqrt{2}(az+1))}{16a^3} - \frac{3q_e^{3/2}\sqrt{\pi}(e^{a^2z^2}-1)e^{2+a^2z_h^2-a^2z^2}\mathrm{erf}(\sqrt{2}(az_h+1))}{16a^3(e^{a^2z_h^2}-1)} - \frac{3\sqrt{\pi}e^{4-a^2z^2}q_e^{3/2}\mathrm{erf}(2+az)}{8\sqrt{2}a^3}, \tag{4.3}$$

which again, under the limit $a \to 0$, reduces to the standard charged BTZ black-hole-like expressions with Coulomb-like potential. In Fig. 12, the behavior of $g(z)$ and the Kretschmann scalar $R_{\mu\nu\rho\sigma}R^{\mu\nu\rho\sigma}$ is illustrated. The spacetime exhibits a horizon at z_h and does not contain any additional singularity, thereby emphasizing the well-behaved nature of the obtained hairy solution. The Ricci scalar is similarly finite and well behaved everywhere outside the horizon. The hair parameter again nontrivially modifies the Kretschmann and Ricci scalars, implying that the spacetime curvature depends nontrivially on the hairy parameter and is no longer a constant. Similarly, the potential asymptotes to a constant value $V(z)|_{z\to 0} = 2\Lambda$ at the AdS boundary and is bounded from above.

Let us now talk about the thermodynamics of this black hole. For the coupling function $f(\phi) = e^{\phi}$, the expression of the black hole temperature is

$$T = \frac{a^2 z_h e^{a^2 z_h^2}}{2\pi(e^{a^2 z_h^2}-1)} + \frac{3q_e^{3/2}z_h e^{a^2z_h^2+4}(\mathrm{erf}(2)-\mathrm{erf}(az_h+2))}{16\sqrt{2\pi}a(e^{a^2z_h^2}-1)} + \frac{3q_e^{3/2}z_h e^{a^2z_h^2+2}(\mathrm{erf}(\sqrt{2}(az_h+1))-\mathrm{erf}(\sqrt{2}))}{32\sqrt{\pi}a(e^{a^2z_h^2}-1)}, \tag{4.4}$$

which also reduces to Eq. (3.8) in the limit $a \to 0$ and to the uncharged BTZ expression in the limit $a \to 0$ and $q_e \to 0$.

Let us again first discuss the black hole thermodynamics in the grand-canonical ensemble. The thermodynamic structure of the hairy black hole with $f(\phi) = e^{\phi}$ coupling remains quite similar to the $f(\phi) = 1$ coupling for the fixed chemical potential ensemble. Notice that for $\mu_e = 0$, the Einstein-power Maxwell-scalar gravity action becomes the same for both $f(\phi) = 1$ and $f(\phi) = e^{\phi}$ couplings, which in turn produces identical thermodynamic structure for both couplings for $\mu_e = 0$. Consequently, for $f(\phi) = e^{\phi}$ coupling as well, there exists a thermodynamically stable hairy black hole phase which undergoes a phase transition to thermal-AdS phase as the temperature is lowered, i.e., the Hawking/page phase transition continues to exist, with the thermal-AdS phase dominating the structure at lower temperatures whereas a large stable hairy black hole phase dominates the phase structure at higher temperatures. For $\mu_e = 0$, the phase diagram is essentially identical to Fig. 3.

The thermodynamic structure with $f(\phi) = e^{\phi}$ coupling remains quite similar to the $f(\phi) = 1$ coupling for the finite chemical potential as well. The results are shown in Figs. 13 and 14. Here again, there exists a critical chemical potential μ_e^c below which the Hawking/Page phase

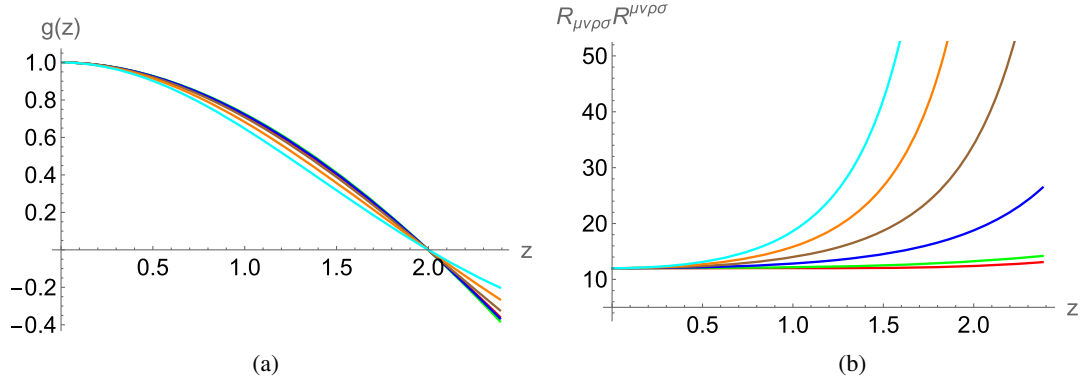

FIG. 12. The nature of $g(z)$ and $R_{\mu\nu\rho\sigma}R^{\mu\nu\rho\sigma}$ for different values of hairy parameter a. Here $z_h = 2.0$ and $q_e = 0.2$ are used. Red, green, blue, brown, orange, and cyan curves correspond to $a = 0, 0.1, 0.2, 0.3, 0.4$, and 0.5, respectively.

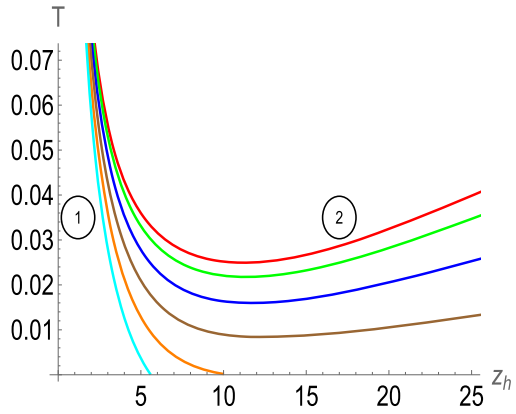

FIG. 13. Hawking temperature T as a function of horizon radius z_h for various values of chemical potential μ_e. Here $a = 0.1$ is used. Red, green, blue, brown, orange, and cyan curves correspond to $\mu_e = 0, 0.2, 0.4, 0.6, 0.8$, and 1.0, respectively.

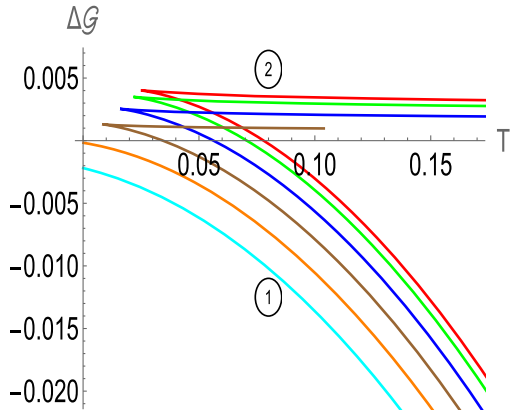

FIG. 14. The Gibbs free energy difference $\Delta\mathcal{G}$ as a function of T for various values of chemical potential μ_e. Here, $a = 0.1$ is used. Red, green, blue, brown, orange, and cyan curves correspond to $\mu_e = 0, 0.2, 0.4, 0.6, 0.8$, and 1.0, respectively.

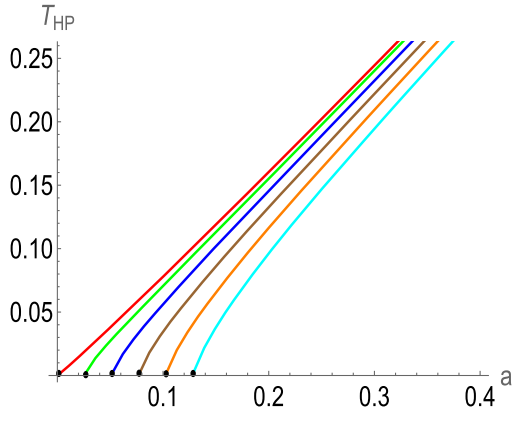

FIG. 15. Hawking/Page phase transition temperature T_{HP} as a function of a for various values of chemical potential μ_e. Red, green, blue, brown, orange, and cyan curves correspond to $\mu_e = 0, 0.2, 0.4, 0.6, 0.8$, and 1.0, respectively. The black dots indicate the critical hairy parameter a_c.

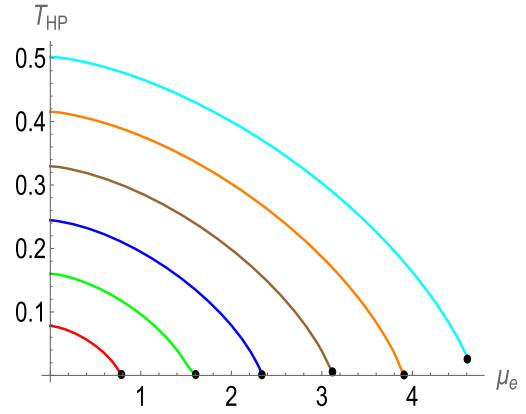

FIG. 16. Hawking/Page phase transition temperature T_{HP} as a function of chemical potential μ_e for various values of a. Red, green, blue, brown, orange, and cyan curves correspond to $a = 0.1, 0.2, 0.3, 0.4, 0.5$, and 0.6, respectively. The black dots indicate the critical chemical potential μ_e^c.

transition between the thermal-AdS and hairy black hole phases take place, whereas no such phase transition appears above μ_e^c. In particular, for $\mu_e < \mu_e^c$, two black hole branches appear which exist only above a certain minimum temperature, whereas, for $\mu_e > \mu_e^c$, only one black hole branch appears which becomes extremal and remain thermodynamically stable at all temperatures. The magnitudes of μ_e^c and the Hawking/Page phase transition T_{HP} again depend nontrivially on the hair parameter a. This dependence is shown in Figs. 15 and 16. The overall behavior of T_{HP} concerning a and μ_e is quite similar to the case of $f(\phi) = 1$, albeit with a different magnitude.

We have similarly analyzed the thermodynamic structure in the canonical ensemble. The temperature and free energy profiles are shown in Figs. 17 and 18. Again, for small

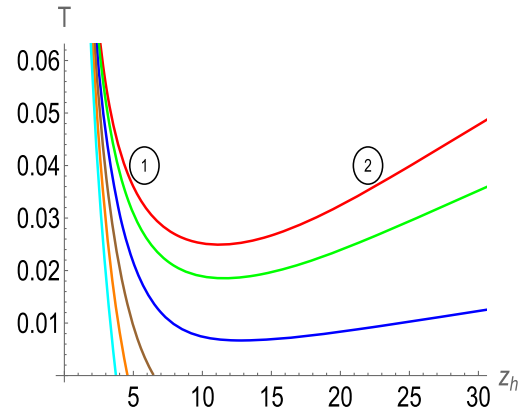

FIG. 17. Hawking temperature T as a function of horizon radius z_h for various values of charge q_e. Here $a = 0.1$ is used. Red, green, blue, brown, orange, and cyan curves correspond to $q_e = 0, 0.1, 0.2, 0.3, 0.4$, and 0.5, respectively.

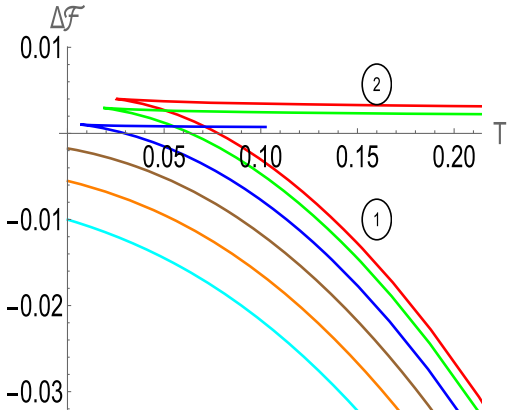

FIG. 18. The Helmholtz free energy difference $\Delta\mathcal{F}$ as a function of T for various values of charge q_e. Here, $a = 0.1$ is used. Red, green, blue, brown, orange, and cyan curves correspond to $q_e = 0, 0.1, 0.2, 0.3, 0.4$, and 0.5, respectively.

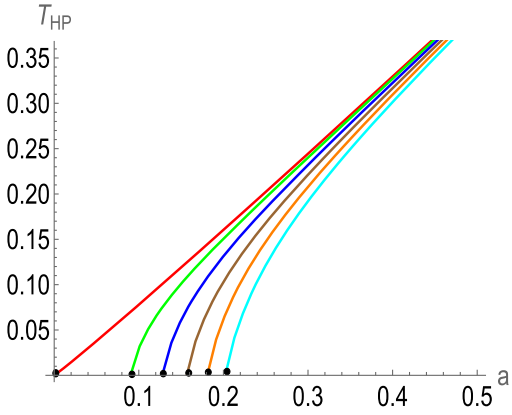

FIG. 19. Hawking/Page phase transition temperature T_{HP} as a function of a for various values of charge q_e. Red, green, blue, brown, orange, and cyan curves correspond to $q_e = 0, 0.2, 0.4, 0.6, 0.8$, and 1.0, respectively. The black dots indicate the critical hairy parameter a_c.

values of q_e, two hairy black hole phases appear, with the large stable hairy black hole phase undergoing phase transition to the thermal-AdS phase as the temperature is lowered, whereas, for relatively large values of q_e, only one stable hairy black hole phase appears which becomes extremal at a certain horizon radius. These results again suggest that, just like in the case of $f(\phi) = 1$, the charged black hole can undergo a Hawking/Page phase transition depending upon the relative magnitude of a and q_e. The structure of T_{HP} again shows monotonic behavior with a and q_e. In particular, T_{HP} increases with a for a fixed q_e, whereas it decreases with q_e for a fixed a. This is shown in Figs. 19 and 20. These results in the canonical ensemble are

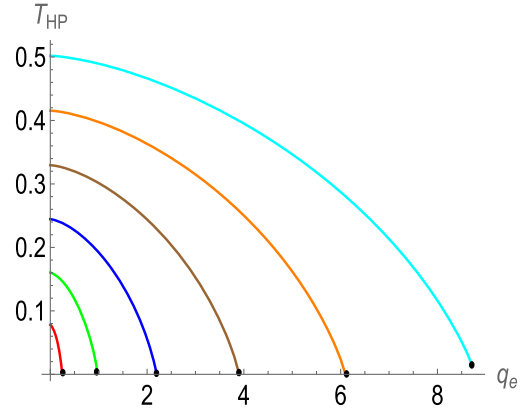

FIG. 20. Hawking/Page phase transition temperature T_{HP} as a function of charge q_e for various values of a. Red, green, blue, brown, orange, and cyan curves correspond to $a = 0.1, 0.2, 0.3, 0.4, 0.5$, and 0.6, respectively. The black dots indicate the critical charge q_e^c.

again quite similar to the $f(\phi) = 1$ coupling, albeit with different magnitudes of T_{HP} and critical values a_c and q_e^c.

V. HAIRY BLACK HOLE SOLUTION WITH COUPLING $f(\phi) = e^{\phi^2/2}$

Now we consider the coupling function $f(\phi) = e^{\phi^2/2}$. Such a coupling function has been thoroughly considered in the hairy black hole context in recent years; see for instance [107]. Therefore, it is instructive to analyze such coupling functions here as well. With $f(\phi) = e^{\phi^2/2}$ coupling, most of our results for the hairy black hole solution remain the same as in the case of previous coupling $f(\phi) = e^{\phi}$. We will, therefore, be brief here. Since the form factor is the same, the solution for the scalar field will remain the same. This implies that the scalar field continues to be regular, finite, and well-behaved everywhere in the exterior horizon region for this exponential coupling function as well. The solution of the gauge field is now given by

$$B_t(z) = \frac{\sqrt{\pi} q_e (\mathrm{erf}(\sqrt{5} a z_h) - \mathrm{erf}(\sqrt{5} a z))}{\sqrt{10} a}, \quad (5.1)$$

with relation between μ_e and q_e as

$$q_e = \sqrt{\frac{10}{\pi}} \frac{a \mu_e}{\mathrm{erf}(\sqrt{5} a z_h)}, \quad (5.2)$$

which has the same $a \to 0$ limit as with the previous coupling functions. The expression for $g(z)$ comes out to be

$$g(z)=\frac{1-e^{a^2(z_h^2-z^2)}}{1-e^{a^2z_h^2}}-\frac{q_e^{3/2}(3\sqrt{10\pi}e^{-a^2z^2}\mathrm{erf}(\sqrt{5}az)-5\sqrt{3\pi}\mathrm{erf}(\sqrt{6}az))}{80a^3}+\frac{q_e^{3/2}\sqrt{\pi}e^{-a^2z^2}(e^{a^2z^2}-1)(3\sqrt{10}\mathrm{erf}(\sqrt{5}az_h)-5\sqrt{3}e^{a^2z_h^2}\mathrm{erf}(\sqrt{6}az_h))}{80a^3(e^{a^2z_h^2}-1)}, \tag{5.3}$$

which reduces to Eq. (3.6) in the $a\to 0$ limit as in the case of previous coupling functions. Therefore, for all different coupling functions considered here, the hairy black hole expressions of various quantities reduce smoothly to the nonhairy expressions in the limit $a\to 0$.

The behavior of $g(z)$ and the Kretschmann scalar for the coupling $f(\phi)=e^{\phi^2/2}$ are shown in Fig. 21. The hairy black hole solution is again regular and well behaved everywhere outside the horizon. The curvature is finite everywhere outside the horizon, and the singularity appears only inside the horizon. The potential similarly asymptotes to a constant value $V(z)|_{z\to 0}=2\Lambda$ at the AdS boundary and is bounded from above. These results firmly establish the well-behaved geometric nature of the hairy black hole with $f(\phi)=e^{\phi^2/2}$ coupling as well.

Let us now briefly talk about the thermodynamics of this black hole. The temperature now has the expression,

$$T=\frac{a^2z_he^{a^2z_h^2}}{2\pi(e^{a^2z_h^2}-1)}+\frac{q_e^{3/2}z_he^{a^2z_h^2}(5\sqrt{3\pi}\mathrm{erf}(\sqrt{6}az_h)-3\sqrt{10\pi}\mathrm{erf}(\sqrt{5}az_h))}{160\pi a(e^{a^2z_h^2}-1)}, \tag{5.4}$$

which also reduces to Eq. (3.8) in the limit $a\to 0$ and to the standard BTZ expression in the limits $a\to 0$ and $q_e\to 0$.

The thermodynamic structure of the hairy black hole in the grand-canonical ensemble is shown in Figs. 22 and 23. Since for $\mu_e=0$, the Einstein-power Maxwell-scalar gravity action becomes identical for all $f(\phi)$, it ensures identical thermodynamic structure for hairy black holes at $\mu_e=0$ for all $f(\phi)$. For $f(\phi)=e^{\phi^2/2}$ and for small chemical potential, there exists a thermodynamically stable hairy black hole phase which undergoes a phase transition to thermal-AdS phase as the temperature is lowered, i.e., the Hawking/Page phase transition continues to exist, with the thermal-AdS phase dominating the structure at lower temperatures. In contrast, a large stable hairy black hole phase dominates the phase structure at higher temperatures. Similarly, there exists a critical chemical potential μ_e^c above which the Hawking/Page phase transition ceases to exist. Therefore, here again for $\mu_e<\mu_e^c$, two black hole branches appear which exist only above a certain minimum temperature, whereas, for $\mu_e>\mu_e^c$, only one black hole branch appears which can become extremal and remain thermodynamically stable at all temperatures. The thermodynamically favored black holes are also thermodynamically stable as they have positive specific heat. The magnitudes of μ_e^c and the Hawking/Page phase transition T_{HP} again depend nontrivially on the hair parameter a. This dependence is shown in Figs. 24 and 25.

The thermodynamic results in the canonical ensemble are shown in Figs. 26 and 27. Here again, we find that depending upon the relative magnitude of a and q_e, the

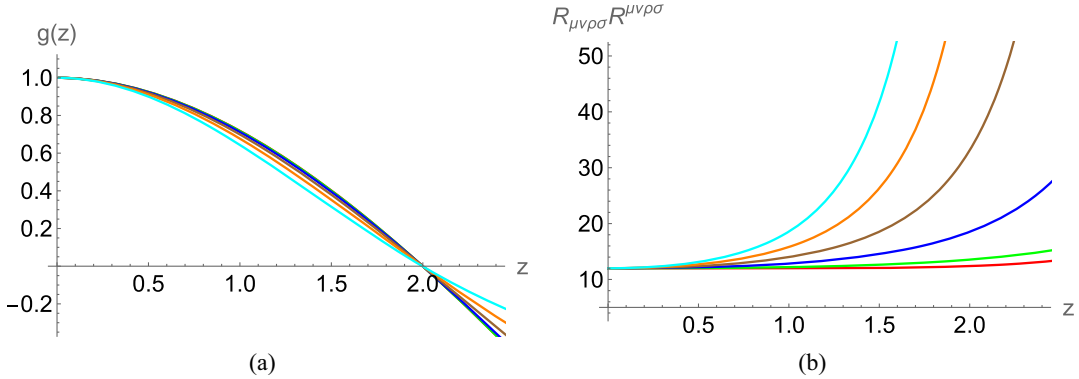

FIG. 21. The nature of $g(z)$ and $R_{\mu\nu\rho\sigma}R^{\mu\nu\rho\sigma}$ for different values of hairy parameter a. Here $z_h=2.0$ and $q_e=0.2$ are used. Red, green, blue, brown, orange, and cyan curves correspond to $a=0, 0.1, 0.2, 0.3, 0.4$, and 0.5, respectively.

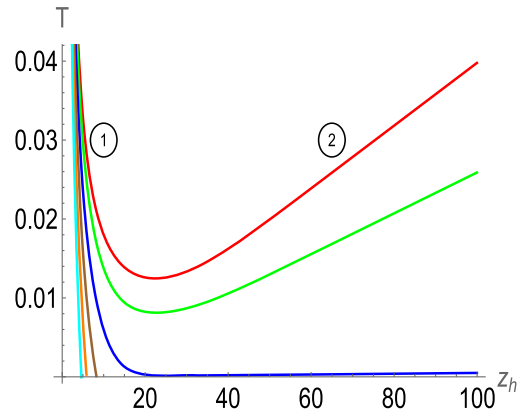

FIG. 22. Hawking temperature T as a function of horizon radius z_h for various values of chemical potential μ_e. Here $a = 0.05$ is used. Red, green, blue, brown, orange, and cyan curves correspond to $\mu_e = 0, 0.2, 0.4, 0.6, 0.8$, and 1.0, respectively.

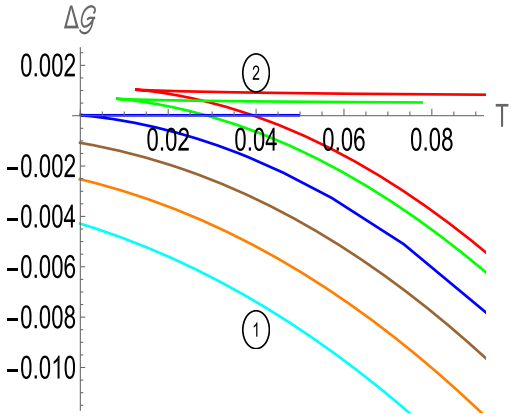

FIG. 23. The Gibbs free energy difference $\Delta\mathcal{G}$ as a function of T for various values of chemical potential μ_e. Here $a = 0.05$ is used. Red, green, blue, brown, orange, and cyan curves correspond to $\mu_e = 0, 0.2, 0.4, 0.6, 0.8$, and 1.0, respectively.

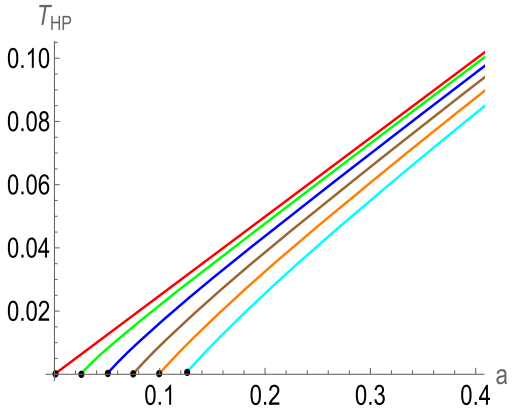

FIG. 24. Hawking/Page phase transition temperature T_{HP} as a function of a for various values of chemical potential μ_e. Red, green, blue, brown, orange, and cyan curves correspond to $\mu_e = 0, 0.2, 0.4, 0.6, 0.8$, and 1.0, respectively. The black dots indicate the critical hairy parameter a_c.

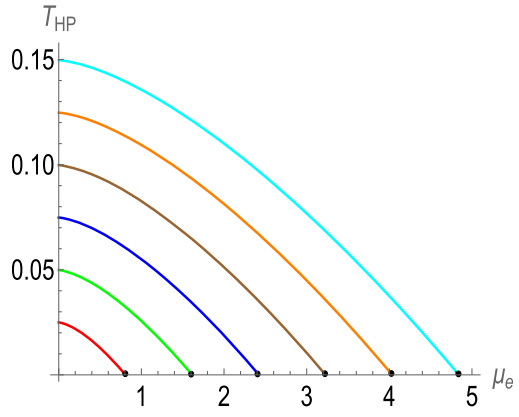

FIG. 25. Hawking/Page phase transition temperature T_{HP} as a function of chemical potential μ_e for various values of a. Red, green, blue, brown, orange, and cyan curves correspond to $a = 0.1, 0.2, 0.3, 0.4, 0.5$, and 0.6, respectively. The black dots indicate the critical chemical potential μ_e^c.

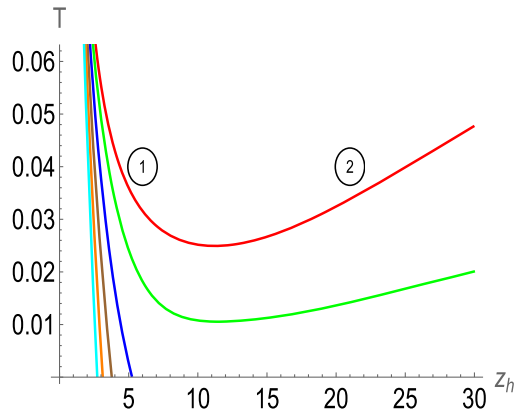

FIG. 26. Hawking temperature T as a function of horizon radius z_h for various values of charge q_e. Here, $a = 0.1$ is used. Red, green, blue, brown, orange, and cyan curves correspond to $q_e = 0, 0.1, 0.2, 0.3, 0.4$, and 0.5, respectively.

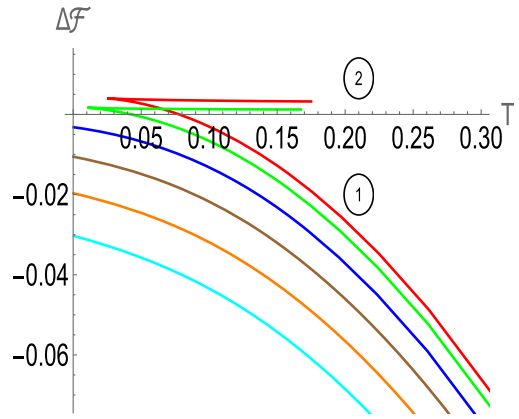

FIG. 27. The Helmholtz free energy difference $\Delta\mathcal{F}$ as a function of T for various values of charge q_e. Here, $a = 0.1$ is used. Red, green, blue, brown, orange, and cyan curves correspond to $q_e = 0, 0.1, 0.2, 0.3, 0.4$, and 0.5, respectively.

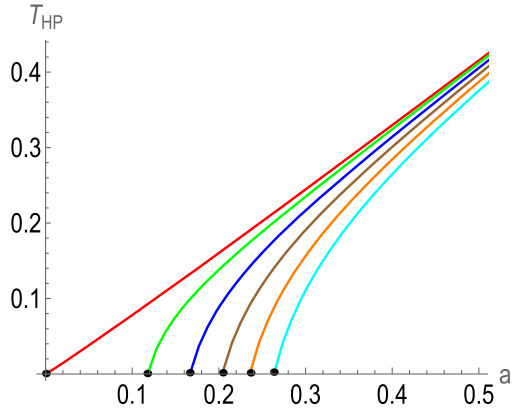

FIG. 28. Hawking/Page phase transition temperature T_{HP} as a function of a for various values of charge q_e. Red, green, blue, brown, orange, and cyan curves correspond to $q_e = 0, 0.2, 0.4, 0.6, 0.8$, and 1.0, respectively. The black dots indicate the critical hairy parameter a_c.

fixed-charged hairy black hole undergoes a Hawking/Page phase transition as the temperature is varied. The corresponding phase transition temperature and critical point q_e^c behavior are illustrated in Figs. 28 and 29.

We end this section by emphasizing that with $f(\phi) = e^{\phi^2/2}$ coupling, the thermodynamic phase diagram of the hairy black hole, both in the canonical and grand-canonical ensemble, remains quite similar to the $f(\phi) = 1$ and $f(\phi) = e^{\phi}$ cases. Our investigation, therefore, indicates some type of universality in the thermodynamic phase structure of the hairy black hole with Coulomb-like potential for different coupling functions. Particularly, there exist critical points $\{\mu_e^c, q_e^c\}$, the magnitude of which are coupling function dependent, below which there appears first-order phase transition between the large hairy black hole and thermal-AdS phases, whereas above these critical points, no such phase transition exits. We analyzed some other forms of $A(z)$ as well and found similar universal results in the thermodynamic phase structure of hairy black holes.

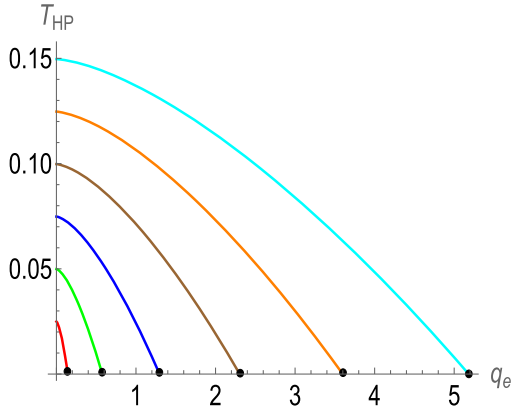

FIG. 29. Hawking/Page phase transition temperature T_{HP} as a function of charge q_e for various values of a. Red, green, blue, brown, orange, and cyan curves correspond to $a = 0.1, 0.2, 0.3, 0.4, 0.5$, and 0.6, respectively. The black dots indicate the critical charge q_e^c.

VI. CONSERVED MASS AND PRIMARY HAIR

In this section, we explicitly show that the obtained three-dimensional hairy black holes are of primary nature. For this purpose, we first compute the conserved charges and show that they depend only on the respective independent integration constants. For the black hole electric charge Q_e, we have already shown that it depends only on the integration constants q_e [Eq. (2.28)]. To show the same for the conserved mass, we need to explicitly evaluate its expression. This can be done using the holographic techniques to construct a Brown-York quasilocal stress tensor [119]. For simplicity, we work in the grand-canonical ensemble, and we concentrate on the simplest $f(\phi) = 1$ case as analogous calculations can be straightforwardly performed in the canonical ensemble as well as for other coupling functions. In the holographic technique, the conserved quantities can be evaluated from the regularized action by adding boundary counterterms. For the gravity system in Eq. (2.1), the same can be computed by subtracting the boundary terms from the bulk on shell action:

$$S_{\text{ren}} = S_{\text{ES}}^{\text{on-shell}} + \frac{1}{8\pi G_3}\int_{\partial\mathcal{M}} \mathrm{d}^2x\sqrt{-\gamma}\Theta - \frac{1}{16\pi G_3}\int_{\partial\mathcal{M}} \mathrm{d}^2x 2\sqrt{-\gamma} + S_b(\phi), \tag{6.1}$$

where the first term is the on shell action, the second term is the Gibbons-Hawking surface term, the third term is the Balasubramanian-Kraus counterterms, and the fourth term is the scalar counterterm. γ is the induced metric on the boundary $\partial\mathcal{M}$, and Θ is the trace of the extrinsic curvature $\Theta_{\mu\nu}$. Note that the variation of the scalar kinetic term contains the boundary term[6]

[6]Depending up on the ensemble there can be additional boundary terms due to the gauge field as well. For instance, the variation of gauge part of the action gives a boundary term $\int_{\partial\mathcal{M}} \mathrm{d}^2x\sqrt{-\gamma}n_r f(\phi)(s\mathcal{F})^{-1/4}F^{r\mu}(\delta B_\mu)$. This term goes to zero in the fixed chemical potential ensemble $\delta B_\mu = 0$. Therefore, this boundary term is not needed in the action for studying thermodynamics in the grant canonical ensemble. However, in the canonical ensemble, corresponding to fixed charge q_e, i.e., $\delta F^{r\mu} = 0$, then the boundary term $\int_{\partial\mathcal{M}} \mathrm{d}^2x\sqrt{-\gamma}n_r(s\mathcal{F})^{-1/4}F^{r\mu}(\delta B_\mu)$ does not vanish, and the term $\int_{\partial\mathcal{M}} \mathrm{d}^2x\sqrt{-\gamma}n_r f(\phi)(s\mathcal{F})^{-1/4}F^{r\mu}B_\mu$ then needs to be added in the action. Also note that the gauge field does not introduce any additional UV divergences in the on shell action as it falls off sufficiently fast near the asymptotic boundary. Therefore, no additional counterterms are needed when $q_e \neq 0$ other than those already present in Eq. (6.3).

$$\delta_\phi S_{\rm ES} = -\frac{1}{16\pi G_3}\int_{\partial\mathcal{M}} \mathrm{d}^2x\sqrt{-\gamma}n^r\partial_r\phi\delta\phi, \tag{6.2}$$

which needs to be added in the action to have a well-defined scalar equation of motion. Therefore, for the scalar counterterm we choose

$$S_b(\phi) = \frac{1}{16\pi G_3}\int_{\partial\mathcal{M}} \mathrm{d}^2x\sqrt{-\gamma}\left(\phi n^r\partial_r\phi + \frac{1}{2}\phi^2\right), \tag{6.3}$$

to make the action well defined [120]. From $S_{\rm ren}$, we can evaluate the stress energy tensor using the Arnowitt-Deser-Misner decomposition

$$T^{\mu\nu} = \frac{1}{8\pi G_3}\left[\Theta\gamma^{\mu\nu} - \Theta^{\mu\nu} + \frac{2}{\sqrt{-\gamma}}\frac{\delta\mathcal{L}_{ct}}{\delta\gamma_{\mu\nu}}\right], \tag{6.4}$$

where $\mathcal{L}_{ct}$ is the Lagrangian of the counterterms only. Explicitly, we have

$$T_{\mu\nu} = \frac{1}{8\pi G_3}\left[\Theta\gamma_{\mu\nu} - \Theta_{\mu\nu} - \gamma_{\mu\nu} + \gamma_{\mu\nu}\left(\frac{\phi}{2}n^r\partial_r\phi + \frac{1}{4}\phi^2\right)\right]. \tag{6.5}$$

The conserved mass of the hairy black hole is then associated to the tt component of the stress tensor. In particular, if K^μ is a Killing vector generating an isometry of the boundary space, then the associated conserved charge is

$$M = \int_\Sigma dx\sqrt{\sigma}u^\mu T_{\mu\nu}K^\nu, \tag{6.6}$$

where Σ is a spacelike surface in $\partial\mathcal{M}$, with induced metric σ, and $u_\mu = -\sqrt{g(z)}\delta^t_\mu$ is the timelike unit normal to Σ.

To compute M and show that it is proportional to the integration constant, let us first write down the metric coefficient $g(z)$ in the following form:

$$g(z) = 1 + \frac{\mathcal{C}e^{-a^2z^2}(e^{a^2z^2}-1)}{2a^2} - \frac{3\sqrt{\pi}e^{-a^2z^2}q_e^{3/2}(\sqrt{2}\mathrm{erf}(az) - e^{a^2z^2}\mathrm{erf}(\sqrt{2}az))}{16a^3}, \tag{6.7}$$

where $\mathcal{C}$ is the integration constant coming from solving Eq. (2.10). Explicitly, we have

$$\mathcal{C} = \frac{2a^2\left(\frac{3\sqrt{\frac{\pi}{2}}q_e^{3/2}(\sqrt{2}\mathrm{erf}(\sqrt{2}az_h) - 2e^{-a^2\mathrm{zh}^2}\mathrm{erf}(az_h))}{16a^3} + 1\right)}{e^{-a^2\mathrm{zh}^2} - 1}. \tag{6.8}$$

Substituting Eq. (6.7) into Eq. (6.6) and simplifying, the hairy black hole mass expression is given by

$$M = -\frac{\mathcal{C}\Omega_1}{32\pi G_3}, \tag{6.9}$$

where $\Omega_1 = 2\pi$ is the unit volume of the boundary space constant hypersurface. We see that M is indeed proportional to the constant $\mathcal{C}$, suggesting that the black hole hair in our cases is of the primary nature. Moreover, this mass expression also matches with the z^2 coefficient of $g(z)$ at the asymptotic boundary, i.e., using the near the boundary expansion of $g(z)$,

$$g(z) = 1 + \frac{\mathcal{C}z^2}{2} + \mathcal{O}(z^3), \tag{6.10}$$

we can show

$$M = -\frac{\Omega_1}{16\pi G_3}\times[z^2\,\text{coefficient of}\,g(z)]. \tag{6.11}$$

Now, substituting the expression of $\mathcal{C}$ into M, we have

$$M = \frac{\Omega_1}{16\pi G_3}\frac{a^2}{1-e^{-a^2z_h^2}}\left(1 + \frac{3\sqrt{\pi}q_e^{3/2}(\sqrt{2}\mathrm{erf}(\sqrt{2}az_h) - 2e^{-a^2z_h^2}\mathrm{erf}(az_h))}{16\sqrt{\pi}a^3}\right), \tag{6.12}$$

which smoothly reduces to the BTZ black hole mass expression $M = \Omega_1/(16\pi z_h^2)$ in the limit $\{a\to 0, q_e\to 0\}$.

From $S_{\rm ren}$, we can further obtain the Gibbs free energy $\mathcal{G} = -S_{\rm ren}/\beta$:

$$\begin{aligned}\mathcal{G} &= \frac{\Omega_1\mathcal{C}}{32\pi G_3},\\ &= -\frac{\Omega_1}{16\pi G_3}\left(\frac{a^2e^{a^2z_h^2}}{e^{a^2z_h^2}-1} + \frac{q_e^{3/2}(3\sqrt{\pi}e^{a^2z_h^2}\mathrm{erf}(\sqrt{2}az_h) - 3\sqrt{2\pi}\mathrm{erf}(az_h))}{16a(e^{a^2z_h^2}-1)}\right)\end{aligned} \tag{6.13}$$

where q_e is given by Eq. (3.4). The above free energy expression also reduces to the BTZ black hole free energy expression in the limit $\{a \to 0, q_e \to 0\}$. Importantly, it also satisfies the expected thermodynamic relation $\mathcal{G} = M - TS_{\rm BH} - Q_e\mu_e$. This provides a nontrivial consistency check for the thermodynamic expressions obtained here for the hairy black holes. Moreover, we further calculated the pressure and find that the standard relation

$$\mathcal{G} = -P \tag{6.14}$$

is also satisfied in the constructed hairy black holes.[7] However, unfortunately, the differential form of the first law is not satisfied in this gravity system. This undesirable result might be correlated to the fact that with hair this form needs to be expanded by additional terms. Indeed, by now many works have advocated for modification of the differential first law in the presence of a scalar field [121,122]. It is of course of great importance to clearly establish the first law in our hairy model; however, since our main aim in this work is on the construction and thermodynamic stability of three-dimensional hairy black holes (and on the corresponding nontrivial phase transitions), we therefore postpone this interesting problem for future work.

Before concluding this section, we would like to emphasize that the near boundary structure of the geometry can be nontrivially modified in the presence of matter fields, especially if they do not fall off reasonably fast at the boundary. This in turn can further modify the conserved charge expression; for instance, see [123,124]. In our hairy-charged gravity model, we too have matter fields that backreact on the geometry; however, importantly they do not change the leading order asymptotic structure of the metric.

VII. CONCLUSIONS

In this paper, we have constructed a new family of three-dimensional hairy-charged black hole solutions from the Einstein-power Maxwell-scalar action. The gauge field solution in particular, being devoid of logarithmic singularity, is everywhere well behaved and reduces to the usual inverse power law behavior for the nonhairy case, thereby downplaying the usual issues faced in Maxwell electrodynamic in three dimensions. The constructed solutions were based on two functions: the coupling function $f(\phi)$ and the form factor $A(z)$. We specifically analyzed the solutions for three interesting and physically motivated forms of the coupling function: (i) $f(\phi) = 1$, (ii) $f(\phi) = e^{\phi}$, and lastly (iii) $f(\phi) = e^{\phi^2/2}$, along with the simple form of $A(z) = -a^2z^2$. The parameter a regulates the strength of the scalar hair, and in the limit $a \to 0$, the solution always reduces to the standard nonhairy BTZ black hole with a Coulomb-like potential. We have observed that in each of the solutions, (i) the scalar hair is found to be regular everywhere outside the horizon and goes to zero at the asymptotic AdS boundary, (ii) the Kretschmann and Ricci scalars are always finite and well behaved outside the horizon, and diverge only at the center of the black hole, and (iii) the potential is found to be bounded from above from its UV boundary value. These results indicate the smooth and desirable nature of the constructed hairy black holes for these different coupling functions.

Next, we analyzed the thermodynamic properties of the hairy black hole solutions in canonical and grand-canonical ensembles and found some universal and intriguing results. For each of the considered coupling functions, a critical value of the hairy parameter a_c appeared above which the black hole exhibited the Hawking/Page phase transition to the thermal-AdS phase as the temperature is lowered, whereas below this a_c no phase transition existed. This result should be contrasted with the usual uncharged BTZ black hole case, where no such phase transition appeared. This suggests that the addition of a scalar hair makes the three-dimensional phase structure much richer. Additionally, it is observed that the associated transition temperature also increases monotonically with a. We similarly analyzed the hairy thermodynamic structure for finite values of q_e and μ_e in the canonical and grand-canonical ensembles and found that the Hawking/Page phase transition continues to persist for small values of q_e and μ_e, whereas for large values of μ_e and q_e no such phase transition occurs. These results indicate the existence of critical values q_e^c and μ_e^c [which are $f(\phi)$ dependent] at which the Hawking/Page phase transition line stops. The transition temperature was further found to be decreasing monotonically with q_e and μ_e. Interestingly, this thermodynamic pattern matches quite well with the charged Reissner-Nordström-AdS black holes in four and higher dimensions. This is intriguing because while BTZ black holes and their counterparts in higher dimensions share a number of geometric characteristics, their thermodynamic structures are very different. We also found that the specific heat is always positive in the thermodynamically favored hairy black hole phase, hence establishing the local stability of the hairy black holes.

This work might be extended in many directions. It would be interesting to extend this work by finding its axisymmetric counterpart. We anticipate that similar to the BTZ black hole, the charged hairy black hole thermodynamic structure may be significantly altered by the rotational parameter. It is also important to check the dynamical stability of the constructed hairy black hole under various perturbations. Our preliminary analysis in this direction leads us to believe that these hairy black holes are dynamically stable under scalar field perturbations. Work in these directions is in progress.

[7] The pressure can be computed from the $\varphi\varphi$ component of $T_{\mu\nu}$.

ACKNOWLEDGMENTS

A. D. would like to express his sincere gratitude to S. Priyadarshinee and S. S. Jena for their insightful discussions throughout the course of this research. The work of S. M. is supported by the Department of Science and Technology, Government of India under the Grant Agreement No. IFA17-PH207 (INSPIRE Faculty Award) and by the core research grant from the Science and Engineering Research Board, Government of India, under Grant Agreement No. CRG/2023/007670.

[1] S. W. Hawking, Particle creation by black holes, Commun. Math. Phys. **43**, 199 (1975); **46**, 206(E) (1976).
[2] G. W. Gibbons and S. W. Hawking, Action integrals and partition functions in quantum gravity, Phys. Rev. D **15**, 2752 (1977).
[3] Jacob D. Bekenstein, Black holes and entropy, Phys. Rev. D **7**, 2333 (1973).
[4] S. W. Hawking and Don N. Page, Thermodynamics of black holes in anti-de Sitter space, Commun. Math. Phys. **87**, 577 (1983).
[5] Andrew Chamblin, Roberto Emparan, Clifford V. Johnson, and Robert C. Myers, Charged AdS black holes and catastrophic holography, Phys. Rev. D **60**, 064018 (1999).
[6] Andrew Chamblin, Roberto Emparan, Clifford V. Johnson, and Robert C. Myers, Holography, thermodynamics, and fluctuations of charged AdS black holes, Phys. Rev. D **60**, 104026 (1999).
[7] Mirjam Cvetic and Steven S. Gubser, Phases of R charged black holes, spinning branes and strongly coupled gauge theories, J. High Energy Phys. 04 (1999) 024.
[8] Anurag Sahay, Tapobrata Sarkar, and Gautam Sengupta, On the thermodynamic geometry and critical phenomena of AdS black holes, J. High Energy Phys. 07 (2010) 082.
[9] Anurag Sahay, Tapobrata Sarkar, and Gautam Sengupta, Thermodynamic geometry and phase transitions in Kerr-Newman-AdS black holes, J. High Energy Phys. 04 (2010) 118.
[10] Anshuman Dey, Subhash Mahapatra, and Tapobrata Sarkar, Thermodynamics and entanglement entropy with Weyl corrections, Phys. Rev. D **94**, 026006 (2016).
[11] Subhash Mahapatra, Thermodynamics, phase transition and quasinormal modes with Weyl corrections, J. High Energy Phys. 04 (2016) 142.
[12] Maximo Banados, Claudio Teitelboim, and Jorge Zanelli, The black hole in three-dimensional space-time, Phys. Rev. Lett. **69**, 1849 (1992).
[13] Máximo Bañados, Marc Henneaux, Claudio Teitelboim, and Jorge Zanelli, Geometry of the $2 + 1$ black hole, Phys. Rev. D **48**, 1506 (1993).
[14] J. David Brown and M. Henneaux, Central charges in the canonical realization of asymptotic symmetries: An example from three-dimensional gravity, Commun. Math. Phys. **104**, 207 (1986).
[15] Juan Martin Maldacena, The large N limit of superconformal field theories and supergravity, Adv. Theor. Math. Phys. **2**, 231 (1998).
[16] Andrew Strominger, Black hole entropy from near horizon microstates, J. High Energy Phys. 02 (1998) 009.
[17] A. Achucarro and P. K. Townsend, A Chern-Simons action for three-dimensional anti-de Sitter supergravity theories, Phys. Lett. B **180**, 89 (1986).
[18] Edward Witten, $(2 + 1)$-dimensional gravity as an exactly soluble system, Nucl. Phys. **B311**, 46 (1988).
[19] Steven Carlip, The $(2 + 1)$-dimensional black hole, Classical Quantum Gravity **12**, 2853 (1995).
[20] Orlando Luongo, Hernando Quevedo, and S. N. Sajadi, Gravitational repulsive effects in 3D regular black holes, Gen. Relativ. Gravit. **56**, 17 (2024).
[21] Seyed Naseh Sajadi, Mohsen Khodadi, Orlando Luongo, and Hernando Quevedo, Anisotropic generalized polytropic spheres: Regular 3D black holes, Phys. Dark Universe **45**, 101525 (2024).
[22] Cristian Martinez, Claudio Teitelboim, and Jorge Zanelli, Charged rotating black hole in three space-time dimensions, Phys. Rev. D **61**, 104013 (2000).
[23] Eric A. Bergshoeff, Olaf Hohm, and Paul K. Townsend, Massive gravity in three dimensions, Phys. Rev. Lett. **102**, 201301 (2009).
[24] Alfredo Perez, David Tempo, and Ricardo Troncoso, Higher spin black hole entropy in three dimensions, J. High Energy Phys. 04 (2013) 143.
[25] Martin Ammon, Michael Gutperle, Per Kraus, and Eric Perlmutter, Spacetime geometry in higher spin gravity, J. High Energy Phys. 10 (2011) 053.
[26] Mauricio Cataldo, Norman Cruz, Sergio del Campo, and Alberto Garcia, $(2 + 1)$-dimensional black hole with Coulomb-like field, Phys. Lett. B **484**, 154 (2000).
[27] Alberto A. García-Díaz, *Exact Solutions in Three-Dimensional Gravity*, Cambridge Monographs on Mathematical Physics (Cambridge University Press, Cambridge, England, 2017).
[28] Alexis Larranaga and Luz Angela Garcia, Thermodynamics of the three-dimensional black hole with a Coulomb-like field, Electron. J. Theor. Phys. **9**, 121 (2012).
[29] Alexis Larranaga, Thermodynamics of the $(2 + 1)$-dimensional black hole with non linear electrodynamics and without cosmological constant from the generalized uncertainly principle, Bulg. J. Phys. **37**, 10 (2010).
[30] Leonardo Balart, Energy distribution of $2 + 1$ dimensional black holes with nonlinear electrodynamics, Mod. Phys. Lett. A **24**, 2777 (2009).
[31] S. Habib Mazharimousavi, O. Gurtug, M. Halilsoy, and O. Unver, $2 + 1$ dimensional magnetically charged solutions

in Einstein-Power-Maxwell theory, Phys. Rev. D **84**, 124021 (2011).
[32] Leonardo Balart and Sharmanthie Fernando, Non-linear black holes in $2+1$ dimensions as heat engines, Phys. Lett. B **795**, 638 (2019).
[33] Ángel Rincón, Ernesto Contreras, Pedro Bargueño, Benjamin Koch, and Grigorios Panotopoulos, Scale-dependent $(2+1)$-dimensional electrically charged black holes in Einstein-power-Maxwell theory, Eur. Phys. J. C **78**, 641 (2018).
[34] Ángel Rincón, Ernesto Contreras, Pedro Bargueño, Benjamin Koch, Grigorios Panotopoulos, and Alejandro Hernández-Arboleda, Scale dependent three-dimensional charged black holes in linear and non-linear electrodynamics, Eur. Phys. J. C **77**, 494 (2017).
[35] M. Dehghani, Thermodynamics of $(2+1)$-dimensional charged black holes with power-law Maxwell field, Phys. Rev. D **94**, 104071 (2016).
[36] Mauricio Cataldo, P. A. González, Joel Saavedra, Yerko Vásquez, and Bin Wang, Thermodynamics of $(2+1)$-dimensional Coulomb-like black holes from nonlinear electrodynamics with a traceless energy momentum tensor, Phys. Rev. D **103**, 024047 (2021).
[37] S. Habib Mazharimousavi, M. Halilsoy, and O. Gurtug, A new Einstein-nonlinear electrodynamics solution in $2+1$ dimensions, Eur. Phys. J. C **74**, 2735 (2014).
[38] P. A. González, Ángel Rincón, Joel Saavedra, and Yerko Vásquez, Superradiant instability and charged scalar quasinormal modes for $(2+1)$-dimensional Coulomb-like AdS black holes from nonlinear electrodynamics, Phys. Rev. D **104**, 084047 (2021).
[39] Z. Amirabi, Generalized Einstein–Power Maxwell theory in $2+1$-dimensions, Eur. Phys. J. Plus **136**, 569 (2021).
[40] Almendra Aragón, P. A. González, Joel Saavedra, and Yerko Vásquez, Scalar quasinormal modes for $2+1$-dimensional Coulomb-like AdS black holes from nonlinear electrodynamics, Gen. Relativ. Gravit. **53**, 91 (2021).
[41] Ahmad Sheykhi, Higher-dimensional charged $f(R)$ black holes, Phys. Rev. D **86**, 024013 (2012).
[42] B. Eslam Panah, M. Khorasani, and J. Sedaghat, Three-dimensional accelerating AdS black holes in F(R) gravity, Eur. Phys. J. Plus **138**, 728 (2023).
[43] Behzad Eslam Panah, Can the power Maxwell nonlinear electrodynamics theory remove the singularity of electric field of point-like charges at their locations?, Europhys. Lett. **134**, 20005 (2021).
[44] S. H. Hendi, B. Eslam Panah, and R. Saffari, Exact solutions of three-dimensional black holes: Einstein gravity versus $F(R)$ gravity, Int. J. Mod. Phys. D **23**, 1450088 (2014).
[45] Gabriel Arenas-Henriquez, Felipe Diaz, and Yerko Novoa, Thermal fluctuations of black holes with non-linear electrodynamics and charged Renyi entropy, J. High Energy Phys. 05 (2023) 072.
[46] Cristian Martinez and Jorge Zanelli, Conformally dressed black hole in $(2+1)$-dimensions, Phys. Rev. D **54**, 3830 (1996).
[47] Marc Henneaux, Cristian Martinez, Ricardo Troncoso, and Jorge Zanelli, Black holes and asymptotics of $2+1$ gravity coupled to a scalar field, Phys. Rev. D **65**, 104007 (2002).
[48] K. C. K. Chan and Robert B. Mann, Static charged black holes in $(2+1)$-dimensional dilaton gravity, Phys. Rev. D **50**, 6385 (1994); **52**, 2600(E) (1995).
[49] Kevin C. K. Chan, Modifications of the BTZ black hole by a dilaton/scalar, Phys. Rev. D **55**, 3564 (1997).
[50] Eloy Ayon-Beato, Cristian Martinez, and Jorge Zanelli, Stealth scalar field overflying a $(2+1)$ black hole, Gen. Relativ. Gravit. **38**, 145 (2006).
[51] Maximo Banados and Stefan Theisen, Scale invariant hairy black holes, Phys. Rev. D **72**, 064019 (2005).
[52] Francisco Correa, Cristian Martinez, and Ricardo Troncoso, Scalar solitons and the microscopic entropy of hairy black holes in three dimensions, J. High Energy Phys. 01 (2011) 034.
[53] Francisco Correa, Aníbal Faúndez, and Cristián Martínez, Rotating hairy black hole and its microscopic entropy in three spacetime dimensions, Phys. Rev. D **87**, 027502 (2013).
[54] Wei Xu and Liu Zhao, Charged black hole with a scalar hair in $(2+1)$ dimensions, Phys. Rev. D **87**, 124008 (2013).
[55] Marcela Cardenas, Oscar Fuentealba, and Cristián Martínez, Three-dimensional black holes with conformally coupled scalar and gauge fields, Phys. Rev. D **90**, 124072 (2014).
[56] Zi-Yu Tang, Yen Chin Ong, Bin Wang, and Eleftherios Papantonopoulos, General black hole solutions in $(2+1)$-dimensions with a scalar field nonminimally coupled to gravity, Phys. Rev. D **100**, 024003 (2019).
[57] M. Dehghani, Thermodynamics of novel charged dilatonic BTZ black holes, Phys. Lett. B **773**, 105 (2017).
[58] M. Dehghani, Thermodynamics of $(2+1)$-dimensional black holes in Einstein-Maxwell-dilaton gravity, Phys. Rev. D **96**, 044014 (2017).
[59] Pablo Bueno, Pablo A. Cano, Javier Moreno, and Guido van der Velde, Regular black holes in three dimensions, Phys. Rev. D **104**, L021501 (2021).
[60] Byoungjoon Ahn, Seungjoon Hyun, Sang-A Park, and Sang-Heon Yi, Scaling symmetry and scalar hairy rotating AdS_3 black holes, Phys. Rev. D **93**, 024041 (2016).
[61] Thanasis Karakasis, Eleftherios Papantonopoulos, Zi-Yu Tang, and Bin Wang, Rotating $(2+1)$-dimensional black holes in Einstein-Maxwell-dilaton theory, Phys. Rev. D **107**, 024043 (2023).
[62] De-Cheng Zou, Yunqi Liu, Bin Wang, and Wei Xu, Thermodynamics of rotating black holes with scalar hair in three dimensions, Phys. Rev. D **90**, 104035 (2014).
[63] J. Sadeghi, B. Pourhassan, and H. Farahani, Rotating charged hairy black hole in $(2+1)$ dimensions and particle acceleration, Commun. Theor. Phys. **62**, 358 (2014).
[64] Moises Bravo-Gaete and Mokhtar Hassaine, Thermodynamics of a BTZ black hole solution with an Horndeski source, Phys. Rev. D **90**, 024008 (2014).
[65] Thanasis Karakasis, George Koutsoumbas, and Eleftherios Papantonopoulos, Black holes with scalar hair in three dimensions, Phys. Rev. D **107**, 124047 (2023).
[66] Remo Ruffini and John A. Wheeler, Introducing the black hole, Phys. Today **24**, No. 1, 30 (1971).

[67] Jacob D. Bekenstein, Nonexistence of baryon number for static black holes, Phys. Rev. D **5**, 1239 (1972).
[68] D. Sudarsky, A simple proof of a no hair theorem in Einstein Higgs theory, Classical Quantum Gravity **12**, 579 (1995).
[69] M. Heusler, A no hair theorem for self-gravitating nonlinear sigma models, J. Math. Phys. (N.Y.) **33**, 3497 (1992).
[70] Carlos A. R. Herdeiro and Eugen Radu, Asymptotically flat black holes with scalar hair: A review, Int. J. Mod. Phys. D **24**, 1542014 (2015).
[71] Werner Israel, Event horizons in static vacuum space-times, Phys. Rev. **164**, 1776 (1967).
[72] Robert M. Wald, Final states of gravitational collapse, Phys. Rev. Lett. **26**, 1653 (1971).
[73] B. Carter, Axisymmetric black hole has only two degrees of freedom, Phys. Rev. Lett. **26**, 331 (1971).
[74] D. C. Robinson, Uniqueness of the Kerr black hole, Phys. Rev. Lett. **34**, 905 (1975).
[75] P. O. Mazur, Proof of uniqueness of the Kerr-Newman black hole solution, J. Phys. A **15**, 3173 (1982).
[76] C. Teitelboim, Nonmeasurability of the quantum numbers of a black hole, Phys. Rev. D **5**, 2941 (1972).
[77] M. S. Volkov and D. V. Galtsov, Black holes in Einstein Yang-Mills theory (In Russian), Sov. J. Nucl. Phys. **51**, 747 (1990).
[78] P. Bizon, Colored black holes, Phys. Rev. Lett. **64**, 2844 (1990).
[79] Brian R. Greene, Samir D. Mathur, and Christopher M. O'Neill, Eluding the no hair conjecture: Black holes in spontaneously broken gauge theories, Phys. Rev. D **47**, 2242 (1993).
[80] P. Kanti, N. E. Mavromatos, J. Rizos, K. Tamvakis, and E. Winstanley, Dilatonic black holes in higher curvature string gravity, Phys. Rev. D **54**, 5049 (1996).
[81] Hugh Luckock and Ian Moss, Black holes have Skyrmion hair, Phys. Lett. B **176**, 341 (1986).
[82] J. Ovalle, R. Casadio, E. Contreras, and A. Sotomayor, Hairy black holes by gravitational decoupling, Phys. Dark Universe **31**, 100744 (2021).
[83] Subhash Mahapatra and Indrani Banerjee, Rotating hairy black holes and thermodynamics from gravitational decoupling, Phys. Dark Universe **39**, 101172 (2023).
[84] Mohsen Dehghani, Three-dimensional black holes with scalar hair coupled to a Maxwell-like electrodynamics, Mod. Phys. Lett. A **37**, 2250205 (2022).
[85] M. Dehghani, Nonlinearly charged three-dimensional black holes in the Einstein-dilaton gravity theory, Eur. Phys. J. Plus **133**, 474 (2018).
[86] M. Dehghani, Three-dimensional scalar-tensor black holes with conformally invariant electrodynamics, Phys. Rev. D **100**, 084019 (2019).
[87] S. H. Hendi, B. Eslam Panah, S. Panahiyan, and A. Sheykhi, Dilatonic BTZ black holes with power-law field, Phys. Lett. B **767**, 214 (2017).
[88] Supragyan Priyadarshinee and Subhash Mahapatra, Analytic three-dimensional primary hair charged black holes and thermodynamics, Phys. Rev. D **108**, 044017 (2023).
[89] Sean A. Hartnoll, Christopher P. Herzog, and Gary T. Horowitz, Holographic superconductors, J. High Energy Phys. 12 (2008) 015.
[90] Jie Ren, One-dimensional holographic superconductor from AdS_3/CFT_2 correspondence, J. High Energy Phys. 11 (2010) 055.
[91] Ling-Yan Hung and Aninda Sinha, Holographic quantum liquids in $1+1$ dimensions, J. High Energy Phys. 01 (2010) 114.
[92] Vijay Balasubramanian, Inaki Garcia-Etxebarria, Finn Larsen, and Joan Simon, Helical Luttinger liquids and three dimensional black holes, Phys. Rev. D **84**, 126012 (2011).
[93] Thomas Faulkner and Nabil Iqbal, Friedel oscillations and horizon charge in 1D holographic liquids, J. High Energy Phys. 07 (2013) 060.
[94] David Dudal and Subhash Mahapatra, Thermal entropy of a quark-antiquark pair above and below deconfinement from a dynamical holographic QCD model, Phys. Rev. D **96**, 126010 (2017).
[95] David J. Gross, Two-dimensional QCD as a string theory, Nucl. Phys. **B400**, 161 (1993).
[96] Supragyan Priyadarshinee, Subhash Mahapatra, and Indrani Banerjee, Analytic topological hairy dyonic black holes and thermodynamics, Phys. Rev. D **104**, 084023 (2021).
[97] Subhash Mahapatra, Supragyan Priyadarshinee, Gosala Narasimha Reddy, and Bhaskar Shukla, Exact topological charged hairy black holes in AdS Space in D-dimensions, Phys. Rev. D **102**, 024042 (2020).
[98] D. Dudal, A. Hajilou, and S. Mahapatra, A quenched 2-flavour Einstein–Maxwell–Dilaton gauge-gravity model, Eur. Phys. J. A **57**, 142 (2021).
[99] Hardik Bohra, David Dudal, Ali Hajilou, and Subhash Mahapatra, Chiral transition in the probe approximation from an Einstein-Maxwell-dilaton gravity model, Phys. Rev. D **103**, 086021 (2021).
[100] Subhash Mahapatra and Pratim Roy, On the time dependence of holographic complexity in a dynamical Einstein-dilaton model, J. High Energy Phys. 11 (2018) 138.
[101] Hardik Bohra, David Dudal, Ali Hajilou, and Subhash Mahapatra, Anisotropic string tensions and inversely magnetic catalyzed deconfinement from a dynamical AdS/QCD model, Phys. Lett. B **801**, 135184 (2020).
[102] Song He, Shang-Yu Wu, Yi Yang, and Pei-Hung Yuan, Phase structure in a dynamical soft-wall holographic QCD model, J. High Energy Phys. 04 (2013) 093.
[103] Irina Aref'eva and Kristina Rannu, Holographic anisotropic background with confinement-deconfinement phase transition, J. High Energy Phys. 05 (2018) 206.
[104] Irina Ya. Aref'eva, Alexey Ermakov, Kristina Rannu, and Pavel Slepov, Holographic model for light quarks in anisotropic hot dense QGP with external magnetic field, Eur. Phys. J. C **83**, 79 (2023).
[105] Irina Ya. Aref'eva, Kristina Rannu, and Pavel Slepov, Holographic anisotropic model for light quarks with confinement-deconfinement phase transition, J. High Energy Phys. 06 (2021) 090.

[106] J. Alanen, K. Kajantie, and V. Suur-Uski, A gauge/gravity duality model for gauge theory thermodynamics, Phys. Rev. D **80**, 126008 (2009).
[107] Carlos A. R. Herdeiro, Eugen Radu, Nicolas Sanchis-Gual, and José A. Font, Spontaneous scalarization of charged black holes, Phys. Rev. Lett. **121**, 101102 (2018).
[108] Steven S. Gubser, Curvature singularities: The good, the bad, and the naked, Adv. Theor. Math. Phys. **4**, 679 (2000).
[109] Sidney R. Coleman, John Preskill, and Frank Wilczek, Quantum hair on black holes, Nucl. Phys. **B378**, 175 (1992).
[110] G. W. Gibbons and Kei-ichi Maeda, Black holes and membranes in higher dimensional theories with dilaton fields, Nucl. Phys. **B298**, 741 (1988).
[111] David Garfinkle, Gary T. Horowitz, and Andrew Strominger, Charged black holes in string theory, Phys. Rev. D **43**, 3140 (1991); **45**, 3888(E) (1992).
[112] P. A. González, Eleftherios Papantonopoulos, Joel Saavedra, and Yerko Vásquez, Four-dimensional asymptotically AdS black holes with scalar hair, J. High Energy Phys. 12 (2013) 021.
[113] Andres Anabalon, Fabrizio Canfora, Alex Giacomini, and Julio Oliva, Black holes with primary hair in gauged $N = 8$ supergravity, J. High Energy Phys. 06 (2012) 010.
[114] Christos Charmousis, Theodoros Kolyvaris, Eleftherios Papantonopoulos, and Minas Tsoukalas, Black holes in bi-scalar extensions of Horndeski theories, J. High Energy Phys. 07 (2014) 085.
[115] Parul Jain, Siddhi Swarupa Jena, and Subhash Mahapatra, Holographic confining-deconfining gauge theories and entanglement measures with a magnetic field, Phys. Rev. D **107**, 086016 (2023).
[116] Bhaskar Shukla, David Dudal, and Subhash Mahapatra, Anisotropic and frame dependent chaos of suspended strings from a dynamical holographic QCD model with magnetic field, J. High Energy Phys. 06 (2023) 178.
[117] Siddhi Swarupa Jena, Bhaskar Shukla, David Dudal, and Subhash Mahapatra, Entropic force and real-time dynamics of holographic quarkonium in a magnetic field, Phys. Rev. D **105**, 086011 (2022).
[118] Peter Breitenlohner and Daniel Z. Freedman, Stability in gauged extended supergravity, Ann. Phys. (N.Y.) **144**, 249 (1982).
[119] Vijay Balasubramanian and Per Kraus, A stress tensor for anti-de Sitter gravity, Commun. Math. Phys. **208**, 413 (1999).
[120] Dumitru Astefanesei, Robert B. Mann, and Raúl Rojas, Hairy black hole chemistry, J. High Energy Phys. 11 (2019) 043.
[121] Hai-Shan Liu and H. Lü, Scalar charges in asymptotic AdS geometries, Phys. Lett. B **730**, 267 (2014).
[122] H. Lu, C. N. Pope, and Qiang Wen, Thermodynamics of AdS black holes in Einstein-scalar gravity, J. High Energy Phys. 03 (2015) 165.
[123] Marc Henneaux, Cristian Martinez, Ricardo Troncoso, and Jorge Zanelli, Asymptotically anti–de Sitter spacetimes and scalar fields with a logarithmic branch, Phys. Rev. D **70**, 044034 (2004).
[124] Marc Henneaux, Cristian Martinez, Ricardo Troncoso, and Jorge Zanelli, Asymptotic behavior and Hamiltonian analysis of anti-de Sitter gravity coupled to scalar fields, Ann. Phys. (Amsterdam) **322**, 824 (2007).